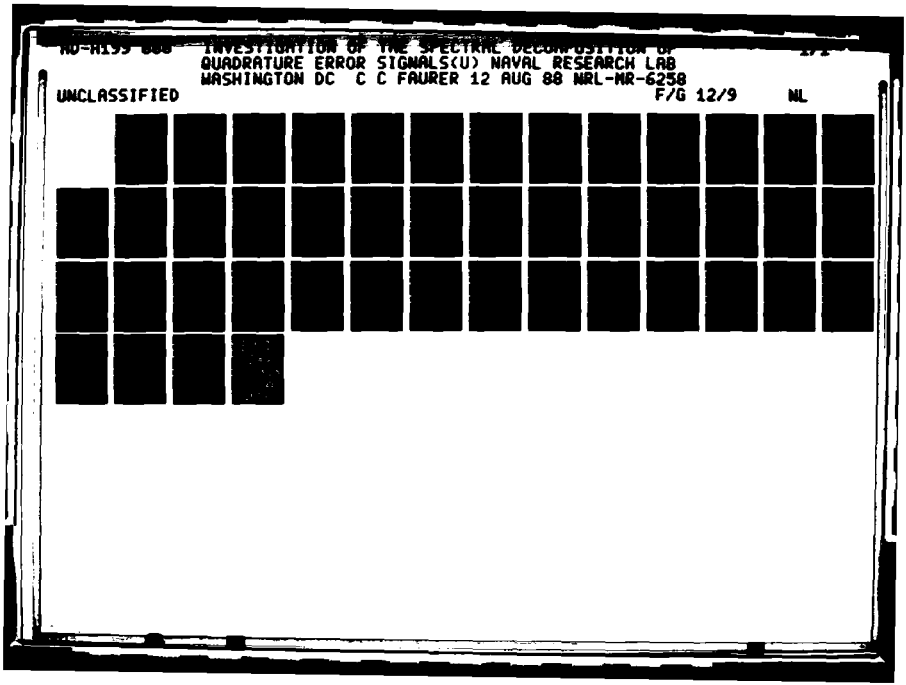
AD-A199 888
INVESTIGATION OF THE SPECTRAL DECOMPOSITION OF
QUADRATURE ERROR SIGNALS(U) NAVAL RESEARCH LAB
WASHINGTON DC C C FAURER 12 AUG 88 NRL-MR-6258
UNCLASSIFIED
F/G 12/9
NL

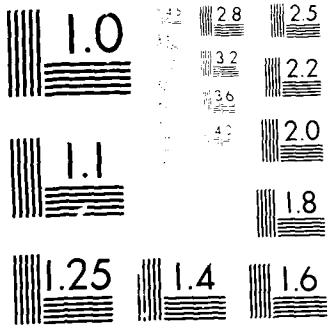
1.0
2.8
2.5
3.2
2.2
3.6
2.0
1.1
1.8
1.25
1.4
1.6

Naval Research Laboratory

Washington, DC 20375-5000

NRL Memorandum Report 6258

Investigation of the Spectral Decomposition of Quadrature Error Signals

C. C. FAURER

Target Characteristics Branch
Radar Division

August 12, 1988

SECURITY CLASSIFICATION OF THIS PAGE

REPORT DOCUMENTATION PAGE

Form Approved
OMB No. 0704-0188

1a. REPORT SECURITY CLASSIFICATION UNCLASSIFIED	1b. RESTRICTIVE MARKINGS
2a. SECURITY CLASSIFICATION AUTHORITY	3. DISTRIBUTION/AVAILABILITY OF REPORT Approved for public release; distribution unlimited.
2b. DECLASSIFICATION/DOWNGRADING SCHEDULE	
4. PERFORMING ORGANIZATION REPORT NUMBER(S) NRL Memorandum Report 6258	5. MONITORING ORGANIZATION REPORT NUMBER(S)
6a. NAME OF PERFORMING ORGANIZATION Naval Research Laboratory	6b. OFFICE SYMBOL (If applicable) Code 5348
6c. ADDRESS (City, State, and ZIP Code) Washington, DC 20375-5000	7b. ADDRESS (City, State, and ZIP Code)
8a. NAME OF FUNDING/SPONSORING ORGANIZATION Chief of Naval Research	8b. OFFICE SYMBOL (If applicable) Code 01124
8c. ADDRESS (City, State, and ZIP Code) Arlington, VA 22217	9. PROCUREMENT INSTRUMENT IDENTIFICATION NUMBER

10. SOURCE OF FUNDING NUMBERS			
PROGRAM ELEMENT NO	PROJECT NO	TASK NO	WORK UNIT ACCESSION NO
62712N		SF12-131-001	DN480-549

11. TITLE (Include Security Classification)
Investigation of the Spectral Decomposition of Quadrature Error Signals

12. PERSONAL AUTHOR(S)
Faurer, C. C.

13a. TYPE OF REPORT	13b. TIME COVERED	14. DATE OF REPORT (Year, Month, Day)	15. PAGE COUNT
Interim	FROM ____ TO ____	1988 August 12	44

16. SUPPLEMENTARY NOTATION

17. COSATI CODES			18. SUBJECT TERMS (Continue on reverse if necessary and identify by block number)
FIELD	GROUP	SUB-GROUP	FFT, Quadrature errors, Band-partitioning

19. ABSTRACT (Continue on reverse if necessary and identify by block number)

This technical report presents the results of an investigation of the performance of band-partitioning filters when the complex signals being transformed contain quadrature errors. Phase and amplitude errors between the in-phase (I) and quadrature-phase (Q) components of a signal can cause significant degradation in the performance of a receiver system. Therefore, it is important to demonstrate how the output of band-partitioning filters, in this case formed by the discrete Fourier transform, are affected by signals with these types of perturbations. Computer simulations are used for this purpose.

Because of the effect of quadrature errors on the system (not described in this report), band partitioning was performed separately on I and Q signal components. In addition to the DFT, Hadamard and Hartley transforms were employed and corresponding responses to swept frequency signals reveal interesting differences.

20. DISTRIBUTION/AVAILABILITY OF ABSTRACT	21. ABSTRACT SECURITY CLASSIFICATION
☒ UNCLASSIFIED/UNLIMITED ☐ SAME AS RPT ☐ DTIC USERS	UNCLASSIFIED
22a. NAME OF RESPONSIBLE INDIVIDUAL Cliff C. Faurer	22b. TELEPHONE (Include Area Code) 202/767-2301 Code 5348

DD Form 1473, JUN 86 Previous editions are obsolete

CONTENTS

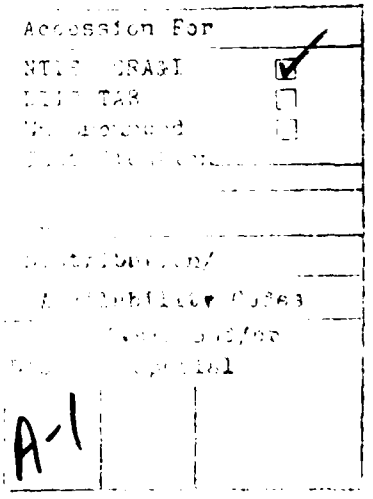

INVESTIGATION OF THE SPECTRAL DECOMPOSITION OF QUADRATURE ERROR SIGNALS

1. Introduction

Two aspects of radar and communications problems are the detection and estimation of received signals. Detection is the process whereby the presence of a received signal is confirmed. Estimation seeks to quantify the detected signal. The process of detection and estimation can be aided by use of a signal processing technique known as spectral decomposition. This process decomposes an observation by a basis set which spans the signal space.[1] One example of this is radar doppler processing, whereby the presence and velocity of a target can be determined. When the particular class of signals being investigated is periodic the choice of a basis set for the decomposition of these signals may lead to the selection of simple periodic functions, the sines and cosines.

The most widely used technique for spectral decomposition based upon this basis set is the Fourier transform. With the discrete Fourier transform (DFT) a set of N uniformly spaced samples of the observed signal are processed. The result is a set of N uniformly spaced harmonic estimates of the signal's periodic spectrum. In practical applications of the DFT the signals of interest are subjected to three operations, sampling, the DFT, and windowing, not necessarily in that order.

The discrete Fourier transform has been examined in some detail and some pitfalls encountered when using the algorithm have been investigated. In particular, work on the problems of aliasing, scalloping loss, and spectral leakage can be found in the literature.[2] This paper examines the special case of spectral decomposition of complex signals containing quadrature error perturbations. Earlier work in this area revealed that a DFT of a complex signal with quadrature errors would generate a false target response located at the mirror image position relative to that of the true target.[3] These results are verified and expanded upon in this paper. Also, the following algorithms are examined for possible use as band-partitioning filters of signals with quadrature errors: the discrete Hartley transform, the Hadamard transform, and the Real DFT. The Real DFT is the term used to describe the discrete Fourier transform of real data.

2. Problem Definition

Many signal processing algorithms require digitized input data to be represented by complex numbers. These complex signals can be derived as part of the receiver detection process by separating real signals into in-phase and quadrature components. In a coherent detector an intermediate frequency signal $A\cos[(\omega_c - \omega_1)t]$ is divided equally between two baseband mixers. These two signals are then mixed with (multiplied by) the two coherent local oscillator signals given by $2\cos\omega_c t$ and $-2\sin\omega_c t$, respectively. The signals exiting from the two mixers are then lowpass filtered to retain only the difference frequency ($\omega_1 \ll \omega_c$) component of the mixing process. The resulting signals are given by

$$I(t) = A\cos\omega_1 t$$

$$Q(t) = A\sin\omega_1 t$$

Manuscript approved June 2, 1988

These signals can be represented as a complex signal by

$$I(t) + jQ(t) = A\, e^{j\omega_1 t}$$

Ideally, for detection, the two channels will differ in phase from one another by 90 degrees and have the same amplitude coefficient. In reality, the phase and amplitude can vary greatly depending upon the quality of the components used to build the receiver and on environmental conditions. These errors are attributable to RF and IF filter response mismatches, RF and IF timedelays, quadrature time delays, mixer phase and amplitude mismatches, and lowpass filter mismatches, to name a few.† For this investigation the errors will be modeled as phase and amplitude errors in the Q channel relative to the I channel. Phase quadrature error is the amount of deviation from the ideal phase separation of 90 degrees between the I and Q channels. The amplitude quadrature error is the difference in gain between the two channels. The quadrature signal equations can now be modified to reflect these errors and are given by

$$I(t) = A\cos\omega_1 t$$

$$Q(t) = (1+\epsilon)A\sin(\omega_1 t - \phi)$$

where

ϵ is the fractional amplitude error,

ϕ is the phase error.

The net effect of these phase and amplitude quadrature errors on a signal's spectrum is to create a false target response at the frequency which is the negative of ω_1. The size of this error response has been quantified by Sinsky and Wang and a technique for correcting these quadrature errors has been proposed by Churchill, Ogar, and Thompson[5] and also by Heydemann.[6] The power of the false image relative to the peak of the ideal response is given approximately by

$$\frac{\epsilon^2}{4} \quad \text{image power (amplitude error)}$$

$$\frac{\phi^2}{4} \quad \text{image power (phase error)}$$

where ϵ is the fractional amplitude error and ϕ is the phase error. Churchill, Ogar, and Thompson give an example of the magnitude of the effects of these two errors. For a gain error of 0.1 dB and a phase error of 1 degree the image power would appear 40 dB below the response of the true target. In practice these two errors can approach 2 degrees in phase and 0.3 dB in amplitude. Errors of this order can cause a measurable degradation in the performance of many signal processing algorithms.

Once a detected signal has been split into I and Q baseband components it is often desirable to perform some type of band-partitioning. The discrete Fourier transform is a classic technique for resolving a sampled waveform into its spectral components. A band-partitioning filter which operates on real valued waveforms is known as the discrete Hartley transform (DHT). Another orthogonalization algorithm to be investigated as a possible transform into the frequency domain is the Hadamard transform. The Hadamard transform is of interest because it can be implemented very easily. Each of the mentioned

† Where analog-to-digital converter speeds permit, these errors can be minimized by direct sampling.[7]

techniques for spectral decomposition can be stated mathematically. The DFT is given by

$$F(\nu) = N^{-1} \sum_{\tau=0}^{N-1} f(\tau)\, e^{\frac{-j2\pi\nu\tau}{N}}, \quad \nu = 0,1,2, \cdots N-1$$

The inverse DFT is given by

$$f(\tau) = \sum_{\nu=0}^{N-1} F(\nu)\, e^{\frac{j2\pi\nu\tau}{N}}, \quad \tau = 0,1,2, \cdots N-1$$

The DHT for real valued sequences is given by

$$F(\nu) = N^{-1} \sum_{\tau=0}^{N-1} f(\tau)\, cas(2\pi\nu\tau), \quad \nu = 0,1,2, \cdots N-1$$

The inverse DHT is given as

$$f(\tau) = \sum_{\tau=0}^{N-1} F(\nu)\, cas(2\pi\nu\tau), \quad \tau = 0,1,2, \cdots N-1$$

where $cas\,\theta = \cos\theta + \sin\theta$

The Hadamard transform is given by

$$\vec{F} = [H]_N \vec{f}$$

$$\vec{f} = N^{-1}[H]_N \vec{F}$$

where $N = 2^k$ $k = 1,2,\ldots$. For example

$$[H]_2 = \begin{vmatrix} + & + \\ + & - \end{vmatrix}$$

and

$$[H]_4 = \begin{vmatrix} + & + & + & + \\ + & - & + & - \\ + & + & - & - \\ + & - & - & + \end{vmatrix}$$

It is interesting to note that both the DHT and the Hadamard transform have the same weighting terms for the forward and inverse directions. In practical terms this could provide a significant savings in hardware since the same weights and even the same algorithm can be used for either the forward or inverse transform.

3. Effect of Quadrature Errors on Band Partitioning

The problem is to find an algorithm which will take a complex input waveform and decompose it into its spectrum and yet be tolerant of quadrature errors. Four algorithms have been given which can be used as band-partitioning filters. It remains to be seen, which one of the four can be used in a system that has I/Q channel perturbations caused by quadrature phase and amplitude errors and still provide a desired level of performance. It has already been noted that the complex DFT will generate a false response which increases as the square of the magnitude of the quadrature errors. This phenomenon will be investigated analytically for any insight it might provide into the behavior of the other transforms. The filters will also be examined by building computer models of each transform and then testing the band-partitioning performance of each algorithm in the presence of phase and amplitude quadrature errors.

A DFT is always used with some type of window weighting of the input data. For the analysis to follow a rectangular window (uniform weighting) is used. By using a rectangular window the frequency domain response of the filter will be realized by the coherent addition of Dirichlet kernels.[7] The first input waveform to be examined is a discrete complex sinusoid given by

$$f(n) = e^{jn\theta_0} \quad \text{where } \theta_0 = \frac{2\pi\nu_0}{N}, \quad n = 0,1,2, \ldots N-1$$

The discrete Fourier transform of this complex waveform is

$$F(\theta) = N^{-1}\sum_{n=0}^{N-1} e^{jn\theta_0}\, e^{-jn\theta} = N^{-1}\sum_{n=0}^{N-1} e^{-jn(\theta-\theta_0)}$$

$$= \frac{1}{N} e^{-j\left|\frac{N-1}{2}\right|(\theta-\theta_0)} \left| \frac{\sin\left|\frac{N}{2}(\theta-\theta_0)\right|}{\sin\left|\frac{1}{2}(\theta-\theta_0)\right|} \right|$$

The result is a single Dirichlet kernel centered about the frequency θ_0 (see Fig. 3). This is the response for a complex sinusoidal input signal if no quadrature errors are present.

A discrete complex cosine signal with phase and amplitude quadrature errors can be represented as follows

$$I(t) = A\cos(n\theta_0)$$

$$Q(t) = (1+\epsilon)A\sin(n\theta_0 - \phi)$$

$$I(t) + jQ(t) = A\cos(n\theta_0) + j(1+\epsilon)A\sin(n\theta_0 - \phi)$$

where

ϵ is the fractional amplitude error.

ϕ is the phase error or sample delay

With each error taken individually and letting A equal unity the error equation becomes

$f_p(n) = \cos(n\theta_0) + j\sin(n\theta_0 - \phi)$ quadrature phase error

$f_a(n) = \cos(n\theta_0) + j(1+\epsilon)\sin(n\theta_0)$ quadrature amplitude error

The DFT of the phase quadrature error complex signal is given as (details in the Appendix)

$$F_p(\theta) = N^{-1}\sum_{n=0}^{N-1}[\cos(n\theta_0) + j\sin(n\theta_0-\phi)]e^{-jn\theta}$$

$$= \frac{1}{N}\sum_{n=0}^{N-1}\cos(n\theta_0)e^{-jn\theta} + \frac{1}{N}\sum_{n=0}^{N-1}j\sin(n\theta_0-\phi)e^{-jn\theta}$$

$$= \frac{1}{2N}e^{-j\left(\frac{N-1}{2}\right)(\theta-\theta_0)}\left|\frac{\sin\left[\frac{N}{2}(\theta-\theta_0)\right]}{\sin\left[\frac{1}{2}(\theta-\theta_0)\right]}\right| + \frac{1}{2N}e^{-j\left(\frac{N-1}{2}\right)(\theta+\theta_0)}\left|\frac{\sin\left[\frac{N}{2}(\theta+\theta_0)\right]}{\sin\left[\frac{1}{2}(\theta+\theta_0)\right]}\right| +$$

$$e^{j\phi}\left|\frac{1}{2N}e^{-j\left(\frac{N-1}{2}\right)(\theta-\theta_0)}\left|\frac{\sin\left[\frac{N}{2}(\theta-\theta_0)\right]}{\sin\left[\frac{1}{2}(\theta-\theta_0)\right]}\right| - \frac{1}{2N}e^{-j\left(\frac{N-1}{2}\right)(\theta+\theta_0)}\left|\frac{\sin\left[\frac{N}{2}(\theta+\theta_0)\right]}{\sin\left[\frac{1}{2}(\theta+\theta_0)\right]}\right|\right|$$

The discrete Fourier transform has revealed an input signal composed of four frequency components, two each at $\pm\theta_0$. The two kernels attributable to the imaginary component of the input signal have a scaling factor which subjects the kernels to a uniform twist. This result was obtained by using the shift theorem which states that a positive shift of a function in time will result in a uniform twist of the spectral components of the signal in frequency. Note that if there is no shifting of the input signal, $\phi=0$, then the spectrum reduces to that derived for the no error case. In fact, the response for the no error case is composed of these four kernels which coherently combine into a single response at θ_0 when $\phi=0$.

The effective spectrum of the phase quadrature error signal is the coherent addition of the four Dirichlet kernels. It can be seen that as ϕ increases the frequency response of the band-partitioning filter will differ markedly from the ideal response. The primary response centered about θ_0 is generated by the addition of two kernels, whereas the image response centered about $-\theta_0$ is generated by the subtraction of two kernels. One of each of the kernels at $\pm\theta_0$ will be twisted by the effect of the time shift. As the twisting increases the kernels at $-\theta_0$ will no longer be matched and the deep null at this frequency will begin to fill in creating an image response of the order $\frac{\phi^2}{4}$. At the frequency $+\theta_0$, the effects of the time shifting will appear as a distortion of the main lobe response (see Fig

The second type of quadrature error results from the unequal gain in the I and Q channels of the receiver. An equation for the amplitude quadrature error signal is

$$\text{amplitude error} = \cos(n\theta_0) + j(1+\epsilon)\sin(n\theta_0)$$

Similar steps are taken to determine the DFT of this signal as were done for the phase error signal (details in the Appendix)

$$F_2(\theta) = N^{-1}\sum_{n=0}^{N-1}[\cos(n\theta_0) + j(1+\epsilon)\sin(n\theta_0)]\,e^{-jn\theta}$$

$$= \frac{1}{N}\sum_{n=0}^{N-1}\cos(n\theta_0)e^{-jn\theta} + \frac{1}{N}\sum_{n=0}^{N-1}j(1+\epsilon)\sin(n\theta_0)e^{-jn\theta}$$

$$= \frac{1}{2N}e^{-j\left[\frac{N-1}{2}\right](\theta-\theta_0)}\left|\frac{\sin\left[\frac{N}{2}(\theta-\theta_0)\right]}{\sin\left[\frac{1}{2}(\theta-\theta_0)\right]}\right| + \frac{1}{2N}e^{-j\left[\frac{N-1}{2}\right](\theta+\theta_0)}\left|\frac{\sin\left[\frac{N}{2}(\theta+\theta_0)\right]}{\sin\left[\frac{1}{2}(\theta+\theta_0)\right]}\right| +$$

$$\frac{(1+\epsilon)}{2N}e^{-j\left[\frac{N-1}{2}\right](\theta-\theta_0)}\left|\frac{\sin\left[\frac{N}{2}(\theta-\theta_0)\right]}{\sin\left[\frac{1}{2}(\theta-\theta_0)\right]}\right| - \frac{(1+\epsilon)}{2N}e^{-j\left[\frac{N-1}{2}\right](\theta+\theta_0)}\left|\frac{\sin\left[\frac{N}{2}(\theta+\theta_0)\right]}{\sin\left[\frac{1}{2}(\theta+\theta_0)\right]}\right|$$

Again the four Dirichlet kernels are seen, however this response differs from that of the phase error signal in two ways. First, the twisting factor due to the time shift is no longer present and second, two of the kernels have scaling factors other than unity. As before, if the error perturbation is not present then the response of the complex signal coherently combines into a single kernel response. The net effect of the amplitude error is the same as for the phase error. A false target will appear at the image frequency of the true target with a magnitude given approximately by $\frac{\epsilon^2}{4}$ (see Fig. 15).

It has been shown that a complex DFT will resolve a quadrature error signal into its spectral components. However, in addition to the desired main response there will be an image frequency response proportional to the amount of quadrature error present in the channels. The image frequency response is caused by one of two things: a twisting of the spectral components due to the time shift caused by the phase error or an amplitude scaling of the kernels caused by the amplitude error. In a complex DFT the coherent addition of the kernels takes place within the transform. To avoid the combining of the quadrature error terms within a single transform a real DFT is used on each of the I and Q channels of the receiver. The disadvantage of this approach is that the complex signal when fed into two real DFT's will transform into four output streams: an I channel, real and imaginary component and a Q channel, real and imaginary component (see Fig 16). The advantage of this approach is that the quadrature error complex signal will be resolved into uncombined spectral terms. That is, the quadrature errors will be isolated within each of the two I and Q channels.

For example, if there are quadrature errors in an input signal then the perturbations will mix across the I and Q channels of all the bands. For an N point DFT, except for the 1st and 4^{th} bands. The response of the second bin of an N point DFT is derived from the input samples as follows:

$$F2_{Re} = I_1 + Q_2 - I_3 - Q_4 + I_5 + Q_6 - I_7 - Q_8$$

$$F2_{Im} = Q_1 - I_2 - Q_3 + I_4 + Q_5 - I_6 - Q_7 + I_8$$

As can be seen, the output of the band will be made up of combinations of I and Q sampled data points. If a quadrature amplitude error a is now introduced into the Q channel the response of the imaginary component of the second bin will be:

$$F2_{Im} = aQ_1 - I_2 - aQ_3 + I_4 + aQ_5 - I_6 - aQ_7 + I_8$$

The error has been dispersed unevenly among the terms and therefore cannot be easily removed from the response. A possible method for combating this problem is to use a real DFT on each of the I and Q channels of the receiver. The real DFT of the I and Q channel data is given as follows:

$$F2I_{Re} = I_1 - I_3 + I_5 - I_7 ; \; F2I_{Im} = -I_2 + I_4 - I_6 + I_8$$

$$F2Q_{Re} = Q_2 - Q_4 + Q_6 - Q_8 ; \; F2Q_{Im} = Q_1 - Q_3 + Q_5 - Q_7$$

The presence of the quadrature amplitude error in the Q channel will cause the Q real and imaginary components to be scaled as shown:

$$F2Q_{Re} = a\left(Q_2 - Q_4 + Q_6 - Q_8\right)$$

$$F2Q_{Im} = a\left(Q_1 - Q_3 + Q_5 - Q_7\right)$$

By transforming each I and Q channel individually as real data it is possible to isolate the quadrature error. After this step, an appropriate signal processing scheme can be used to compensate for these errors. A more general discussion of the DFT of real data follows.

The real DFT of the discrete complex waveform is accomplished by transforming each channel individually. The real part of the discrete complex input waveform is

$$x(n) = \cos(n\theta_0), \quad n = 0,1,2, \qquad N-1$$

The real DFT of this signal is

$$X(0) = N^{-1} \sum_{n=0}^{N-1} \cos(n\theta_0) e^{-j2\pi}$$

$$= \frac{1}{2N} \sum_{n=0}^{N-1} e^{j2\pi(1)n - j2\pi n} + \frac{1}{2N} \sum_{n=0}^{N-1} e^{-j2\pi(1)n - j2\pi n}$$

$$= \frac{1}{2N}\sum_{n=0}^{N-1} \qquad - \frac{1}{2N}\sum_{n=0}^{N-1}$$

$$= \frac{1}{2N} e^{-\frac{N-1}{2}(\theta-\theta_0)} \left| \frac{\sin\left|\frac{N}{2}(\theta-\theta_0)\right|}{\sin\left|\frac{1}{2}(\theta-\theta_0)\right|} \right| + \frac{1}{2N} e^{-\frac{N-1}{2}(\theta+\theta_0)} \left| \frac{\sin\left|\frac{N}{2}(\theta+\theta_0)\right|}{\sin\left|\frac{1}{2}(\theta+\theta_0)\right|} \right|$$

The spectrum consists of two kernels centered about $\pm\theta_0$. These are the same kernels as those obtained with the complex DFT. The difference is that the kernels are presented as the real and imaginary parts of the transform of the I channel of the receiver.

The portion of the phase quadrature error waveform in the Q channel of the receiver was given by

$$f_2(n) = j\sin(n\theta_0 + \phi)$$

The real DFT of this signal is

$$F_2(\theta) = N^{-1}\sum_{n=0}^{N-1} j\sin(n\theta_0+\phi)\, e^{-jn\theta}$$

$$= je^{-j\phi}\left[\frac{1}{j2N}\sum_{n=0}^{N-1} e^{jn\theta_0}e^{-jn\theta} - \frac{1}{j2N}\sum_{n=0}^{N-1} e^{-jn\theta_0}e^{-jn\theta}\right]$$

$$= e^{-j\phi}\left[\frac{1}{2N}\sum_{n=0}^{N-1} e^{-jn(\theta-\theta_0)} - \frac{1}{2N}\sum_{n=0}^{N-1} e^{-jn(\theta+\theta_0)}\right]$$

$$= e^{-j\phi}\left[\frac{1}{2N} e^{-j\frac{N-1}{2}(\theta-\theta_0)} \left| \frac{\sin\left|\frac{N}{2}(\theta-\theta_0)\right|}{\sin\left|\frac{1}{2}(\theta-\theta_0)\right|} \right| - \frac{1}{2N} e^{-j\frac{N-1}{2}(\theta+\theta_0)} \left| \frac{\sin\left|\frac{N}{2}(\theta+\theta_0)\right|}{\sin\left|\frac{1}{2}(\theta+\theta_0)\right|} \right|\right]$$

Again the two kernels are the same as those obtained by using the complex DFT. By using the real DFT and band-partitioning each I and Q channel separately the resulting kernels are not coherently combined into a single complex response. Instead the isolation between the two input channels is maintained and therefore the quadrature errors are not mixed across real and imaginary bands. A similar derivation can be done for the amplitude quadrature error signal with comparable results.

The Hartley and Hadamard transforms will not be examined analytically. Instead their frequency response will be examined and compared with that obtained for the DFT by using a digital computer to implement each band-partitioning filter. The scenario for this investigation is shown in Figure 12. The continuous waveform (CW) signal source is also modeled in the computer and allows the generation of any complex or real valued signal with variable amplitude and phase quadrature errors.

4. Computer Results

The results obtained analytically for the spectral decomposition of a quadrature error signal can be verified graphically by using the computer. The band partitioning filters are examined in the following order: the complex DFT, the real DFT, the DHT, and the Hadamard transform. The DHT and Hadamard transform are being investigated because they are both real one port operations which can be built to run faster than the FFT.[3,4] If they have satisfactory band-partitioning characteristics they can be used instead of the real DFT for decomposing a complex signal into spectral components.

The DFT of a complex valued cosinusoidal signal should produce a single Dirichlet kernel response at the frequency of the input waveform. In Figure (3) the response of the second bin ($k=2$) of an 8 point DFT is shown. This plot is obtained by injecting a complex cosine waveform is swept in frequency from $-\frac{f_s}{2}$ to $\frac{f_s}{2}$) into the 8 point complex DFT. For the values selected, bin 2 should have its peak response at $\frac{f_s}{4}$ and that is what is seen in the figure. The shape of the kernel is determined by the weight applied to the sampled data. For this investigation a rectangular weight is used and this is confirmed by the -13 dB sidelobes. The overlay of all of the 8 bands is shown in Figure (4). This plot shows that a complex DFT will decompose an input waveform into 8 filter banks each centered about the frequency $k\frac{f_s}{N}$ where f_s is the sample frequency and N is the number of points in the DFT. The index k runs from $-\frac{N}{2}$ to $\frac{N}{2}$. This is the band-partitioning filter response for complex valued waveforms.

A phase quadrature error of 10 degrees is now introduced into the complex input signal. The frequency response of all eight bins is shown in Figures (5-12). The frequency response of the second bin of the complex DFT is shown in Figure (7). The false target response is clearly visible at the image frequency. A comparison with Figure (3) shows that the response at the image frequency should be a deep null and not a -20 dB response. The reason for the change in the response of the complex DFT is that the coherent addition of the four Dirichlet kernels no longer results in a single kernel. The quadrature error of 10 degrees has caused the spectral components of the kernel to be twisted uniformly with frequency. This twisting of the frequency response is due to the time delay caused by the phase error. Recall that at $+\theta_0$ the two kernels add together and at $-\theta_0$ the kernels subtract. The result of this twisting of the kernels is most noticeable at the image frequency. While there may not be a noticeable change in the shape of the response at the primary frequency it is occurring.

The amplitude quadrature error will produce a similar change in the complex DFT's frequency response. The frequency response of all the bins is shown in Figures (13-20). For these plots the amplitude of the Q channel is twice that of the I channel. The DFT of the amplitude quadrature error signal results in four Dirichlet kernels centered about $\pm\theta_0$ where two of the kernels have scaling factors proportional to the amplitude error. The response of the second bin of the DFT is shown in Figure (15). Again the false target response is seen to be present centered about the image frequency. The result of coherently adding the four mismatched kernels is seen to affect the overall response of the filter bank. The change in the shape of the mainlobe and sidelobes of the target is quite visible.

The results obtained with the computer agree with those obtained analytically. The mathematical results revealed the mechanics of what occurs within a complex DFT. The computer plots provide visual evidence of the net result of coherently combining the four Dirichlet kernels. The frequency response of the real DFT (recall that this is the DFT of real data) will be examined next.

The real DFT is applied to the I channel of the receiver and the output of bin 2 is shown in Figure (21). This display differs from that seen for the complex DFT. The real DFT produces two kernels centered about $\pm\theta_0$ instead of the four seen with the complex DFT. The net response of the complex DFT was a single kernel centered about θ_0 because of the way in which the four kernels coherently combined within the transform. In the real DFT there are no opposing kernels centered about $-\theta_0$; there is only one kernel as can be seen in Figure (21). The overall frequency response of the filter bank is the result of the coherent addition of these two kernels. The overlay of all the filter bank responses is shown in Figure (22). It can be seen that the overall response maintains the symmetry seen to be present in the complex DFT.

The transform of the Q channel of the receiver will produce plots similar to those already seen for the I channel. The effect of the phase quadrature error will be to rotate the real and imaginary vectors about their axis.[10] The magnitude response will appear to be the same at each phase error step. The amplitude quadrature error will scale the response of the filter by an amount proportional to the error.

The disadvantage of using the real DFT for spectral decomposition is that it creates a two-in four-out type of network (see Fig 1). However, it has been shown that this approach will decompose a quadrature error complex valued signal into its periodic spectrum. If it is preferable to maintain the two-in two-out configuration then the discrete Hartley transform and Hadamard transform will satisfy this requirement. It remains to be seen if these two algorithms are able to band-partition a time domain signal as well as the real DFT.

The DHT has been suggested as an alternative to the real DFT for several reasons. The primary reason is the savings in compute time afforded by the single set of weights needed for both directions of the transform. The same is true for the Hadamard transform. The response of the second bin of the discrete Hartley transform for the cosine input waveform is shown in Figure (23). For the real DFT of the same input waveform the mainlobe was centered about $\frac{f_s}{4}$. For the DHT, the mainlobe is not centered about $\frac{f_s}{4}$ and is not symmetrical. The same type of behavior is exhibited by the other bands as well. The overlay of all these filters is shown in Figure (24). The DHT may be useful as a mathematical alternative to the real DFT but it does not have much merit as a band-partitioning filter.

The last filter to be examined is the Hadamard transform. This algorithm is very easily implemented due to the simplicity of the weighting terms. As with the DHT the same weights are used for the forward and inverse transforms. The Hadamard weights are either +1 or -1. The DHT and the Hadamard transform have similar behavior. In fact, if $N = 4$ then the two transforms are identical.

The filter bank which has been the focus of this discussion happens to be one of the banks which the DHT and Hadamard transform have in common. This can be seen by comparing the response of the second bin of the Hadamard transform shown in Figure

25) with that for the DHT as seen in Figure 23). The overall response of the Hadamard transform is shown in Figure(26). A comparison with the total response of the DHT will highlight the similarities between these two algorithms. Unfortunately, the Hadamard transform also exhibits the poor band-partitioning performance seen with the DHT.

5. Conclusions

This investigation was undertaken to examine the behavior of four band-partitioning filters. The complex DFT and real DFT were analyzed mathematically in order to obtain a better understanding of the mechanics of each algorithm. In the complex DFT the spectral components of the signal are coherently combined internal to the transform. This process can be avoided by using using two real DFT's to filter the same input signal and thus keep the I and Q channel data separated. The Hartley and Hadamard transforms were investigated by developing computer models of each algorithm and then testing each filter.

The complex DFT has been widely used as a band-partitioning filter in many digital signal processing systems. As others have shown, there are problems with using this filter in receiver systems with quadrature errors. The most significant effect of I/Q channel quadrature error is to cause a false image response to appear at a frequency which is the negative of the frequency of the target response. This behavior of the complex DFT was verified both mathematically and graphically. It is because of this perturbation of the signal spectrum, caused by the mixing of the quadrature errors between the real and imaginary components of the spectrum, that the complex DFT makes a poor band-partitioning filter under these conditions.

The Hartley and Hadamard transforms operate on real data. Each algorithm uses a single set of weights to transform between the two domains of time and frequency. By using only a single set of weights less memory is required for storage when these filters are implemented in hardware. The basis set for the Hartley transform is given by $cas\,\theta = \cos\theta + \sin\theta$. For the Hadamard transform the basis set is quite simple, the values ± 1. Even though each of these transforms can be efficiently implemented and do provide the desired quadrature separation they do not make good band-partitioning filters. The reason for this is that the input signals of interest are composed of sines and cosines and the Hadamard transform basis set is not made up of these waveforms.

When the data from the I and Q channels of a receiver are transformed, using the DFT, as two real numbers instead of a single complex number then the desired band-partitioning filter is obtained. The difference is that by using quadrature separation, channel mismatches can be isolated to a particular spectral component. By doing this, succeeding digital signal processing techniques can be used to compensate for these channel mismatch errors and thereby achieve a desired level of system performance.

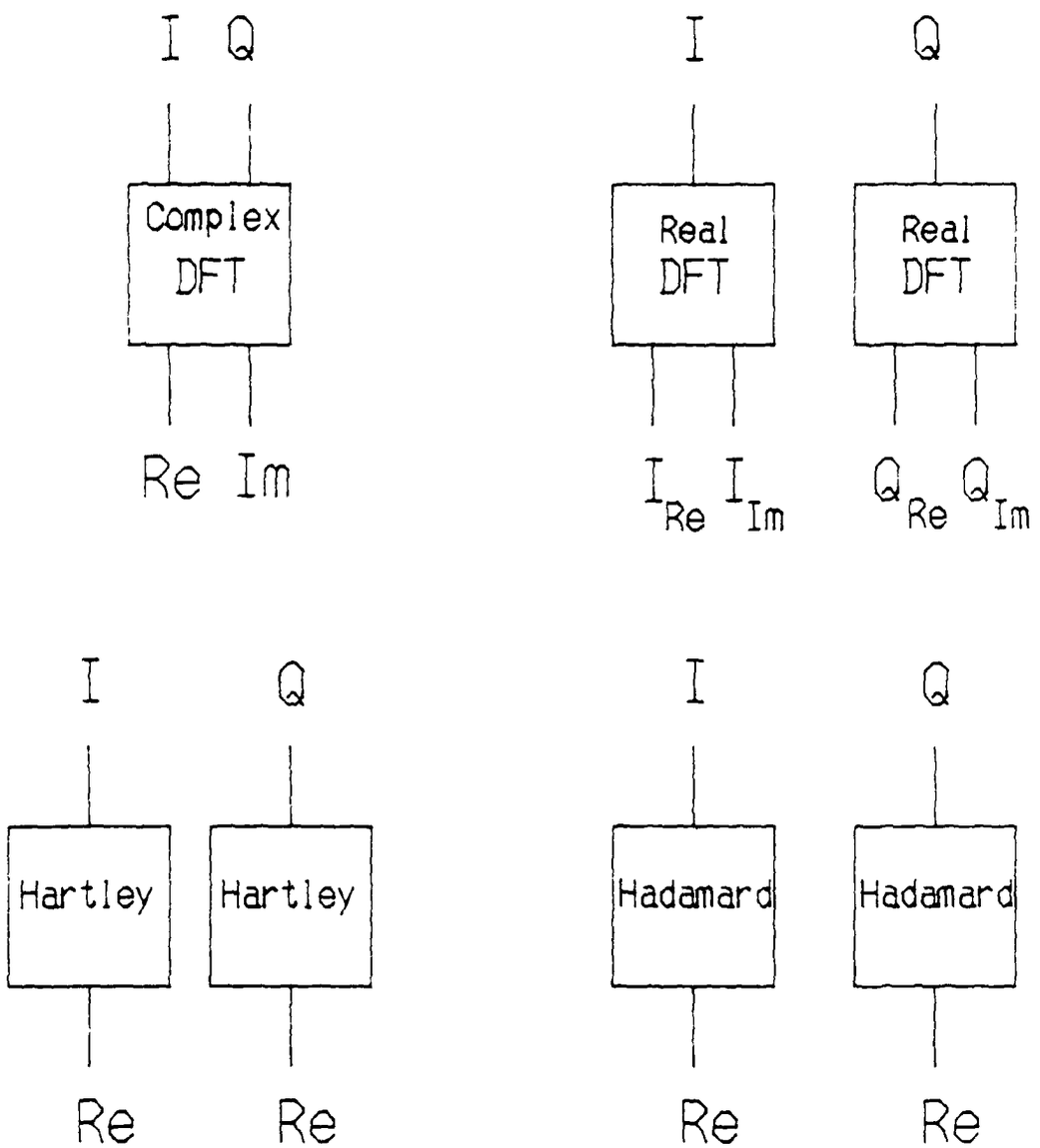

Fig. 1 — Bandpartitioning Filter Configurations

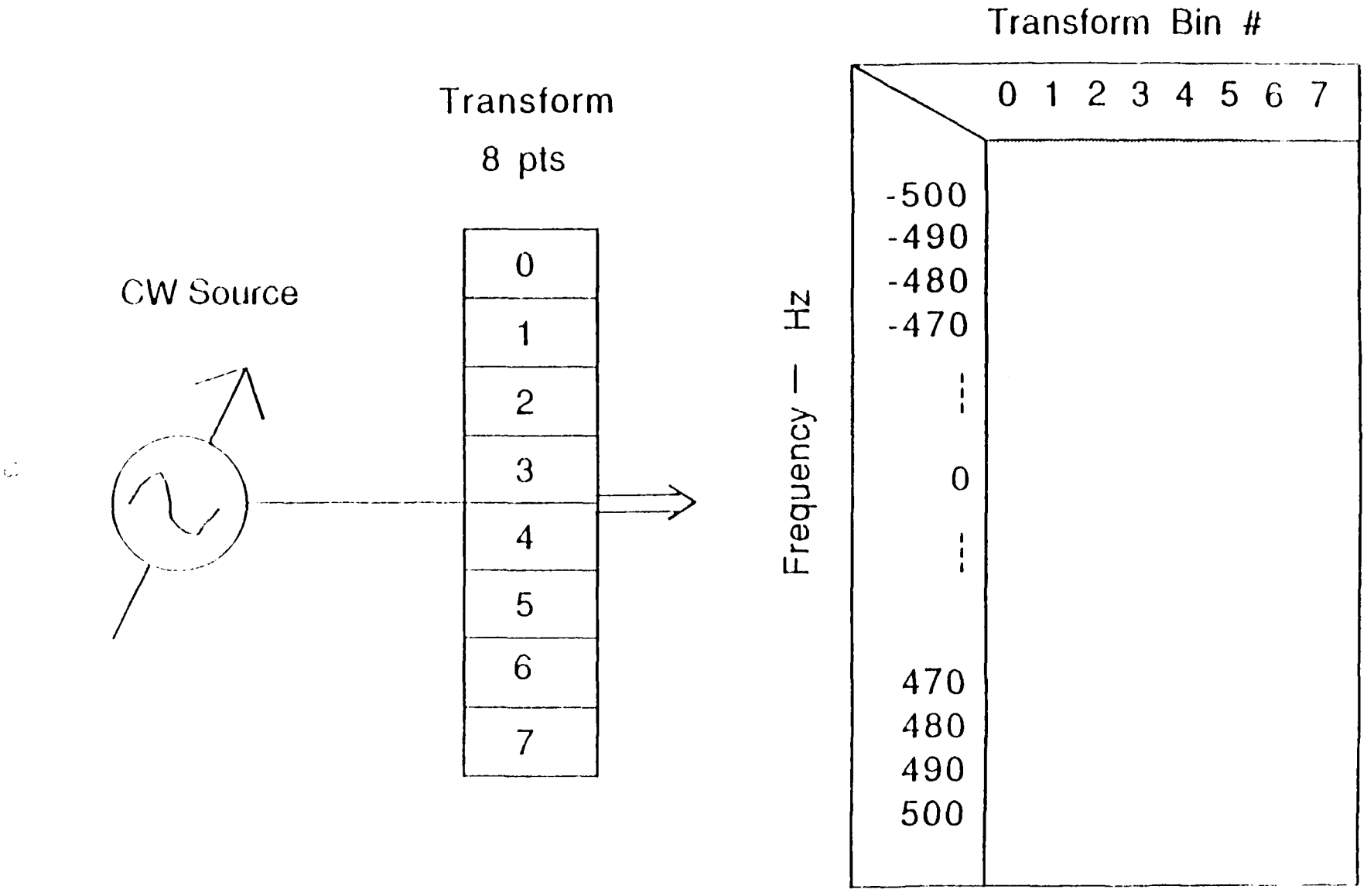
Transform Bin #
0 1 2 3 4 5 6 7
Transform
8 pts
CW Source
0
1
2
3
4
5
6
7
Frequency — Hz
-500
-490
-480
-470
0
470
480
490
500

Figure 2

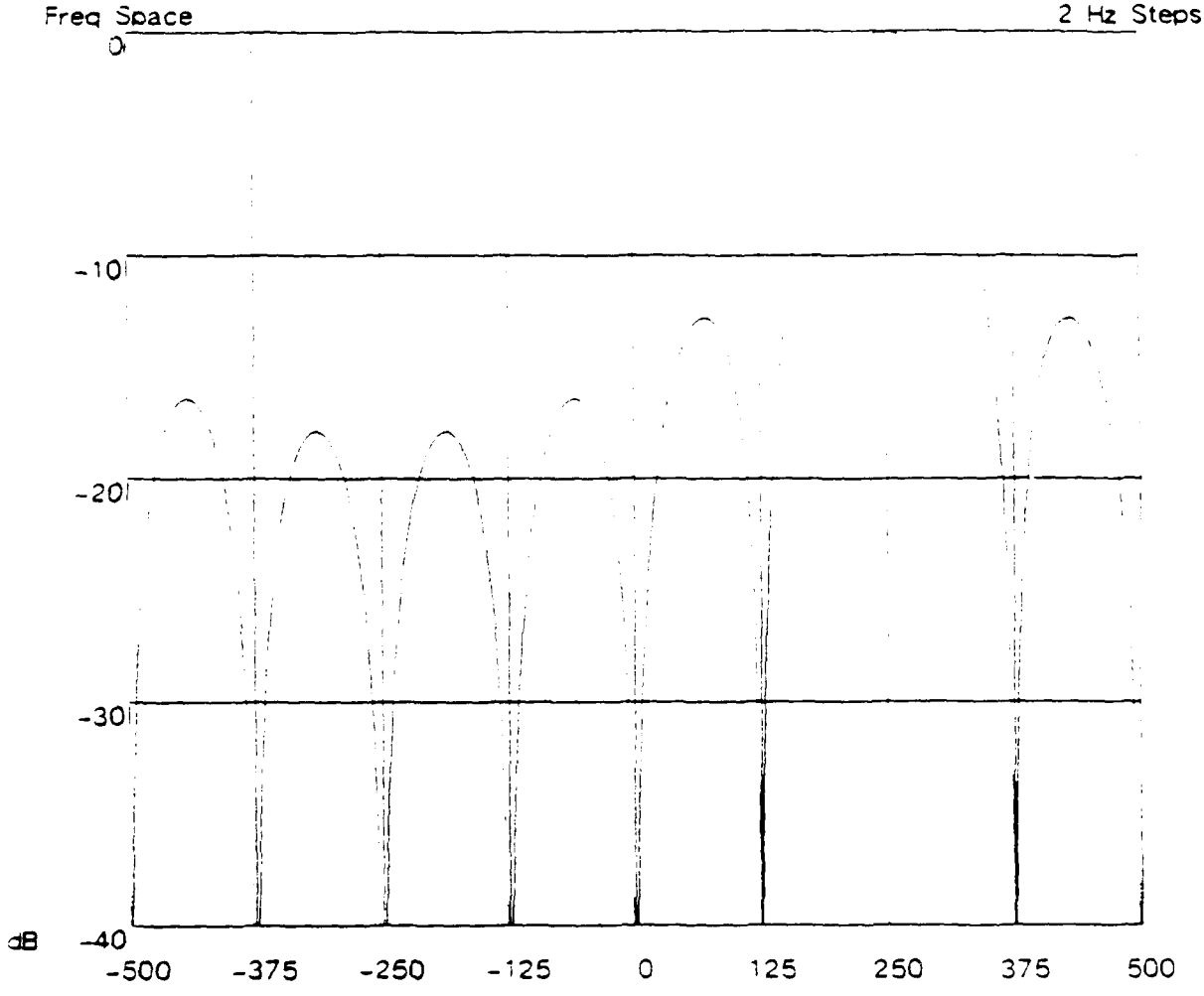

Complex FFT Bin 2

Figure 3

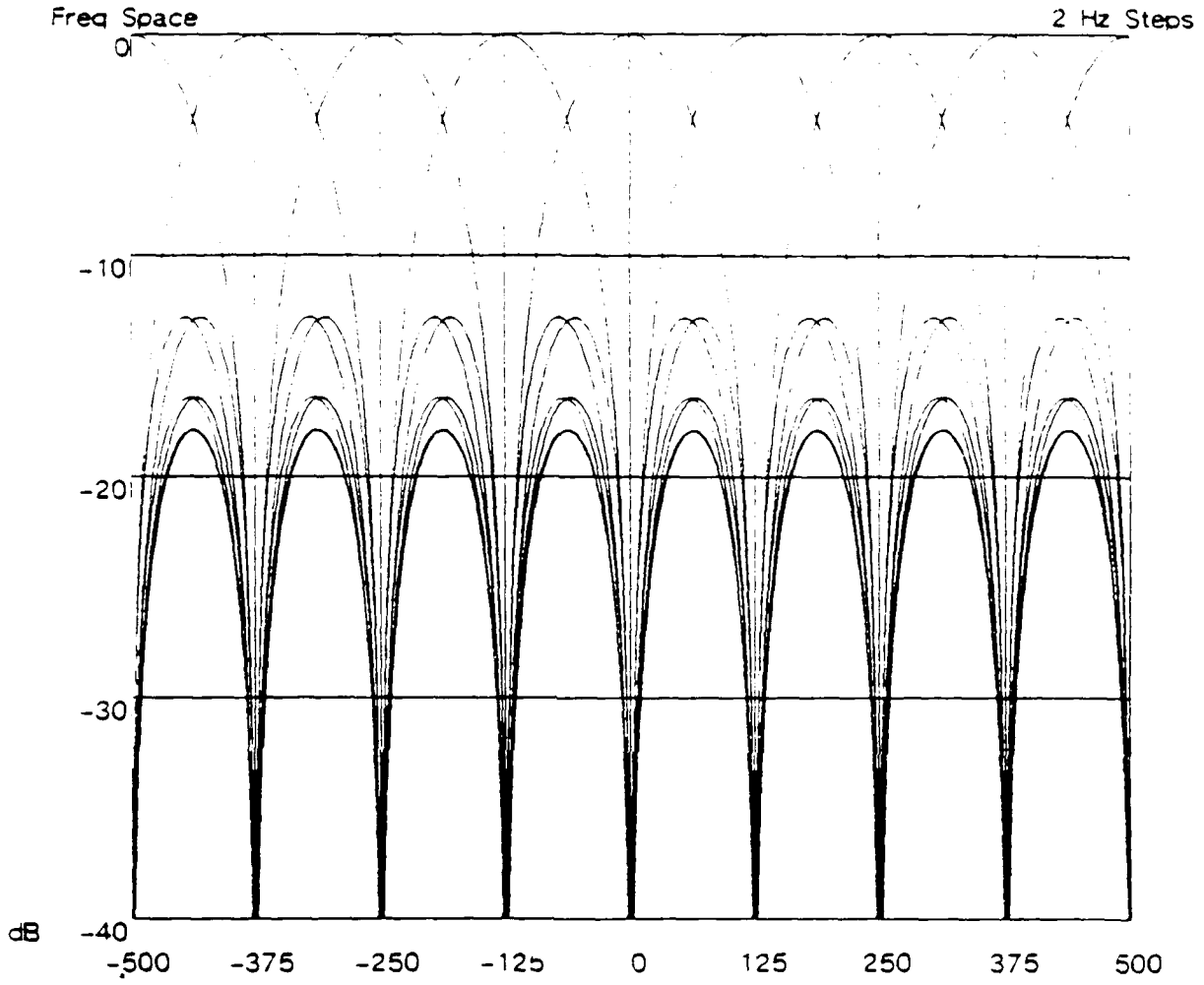

Complex FFT

Figure 4

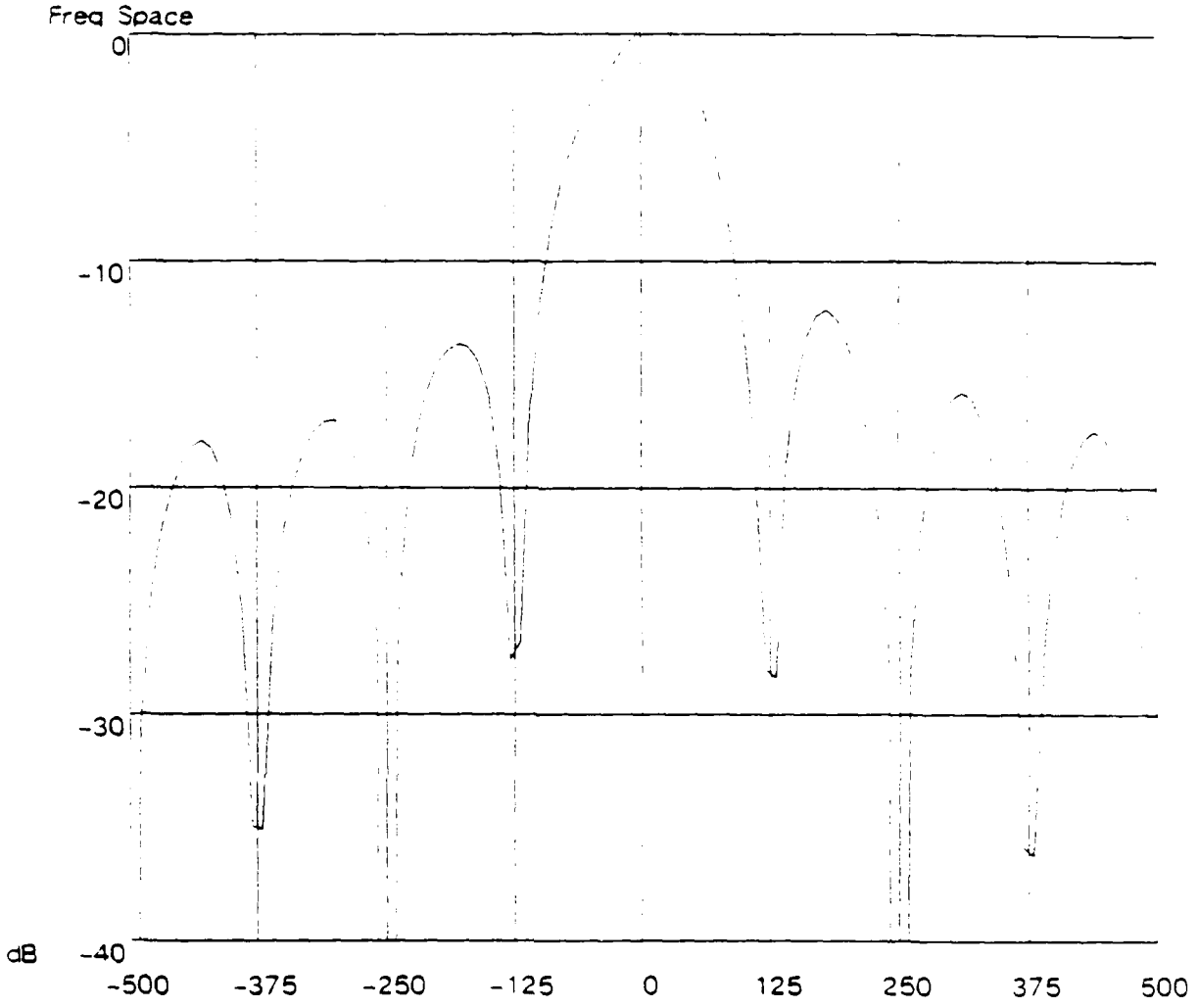

FFT qe=10 Bin 0

Figure 5

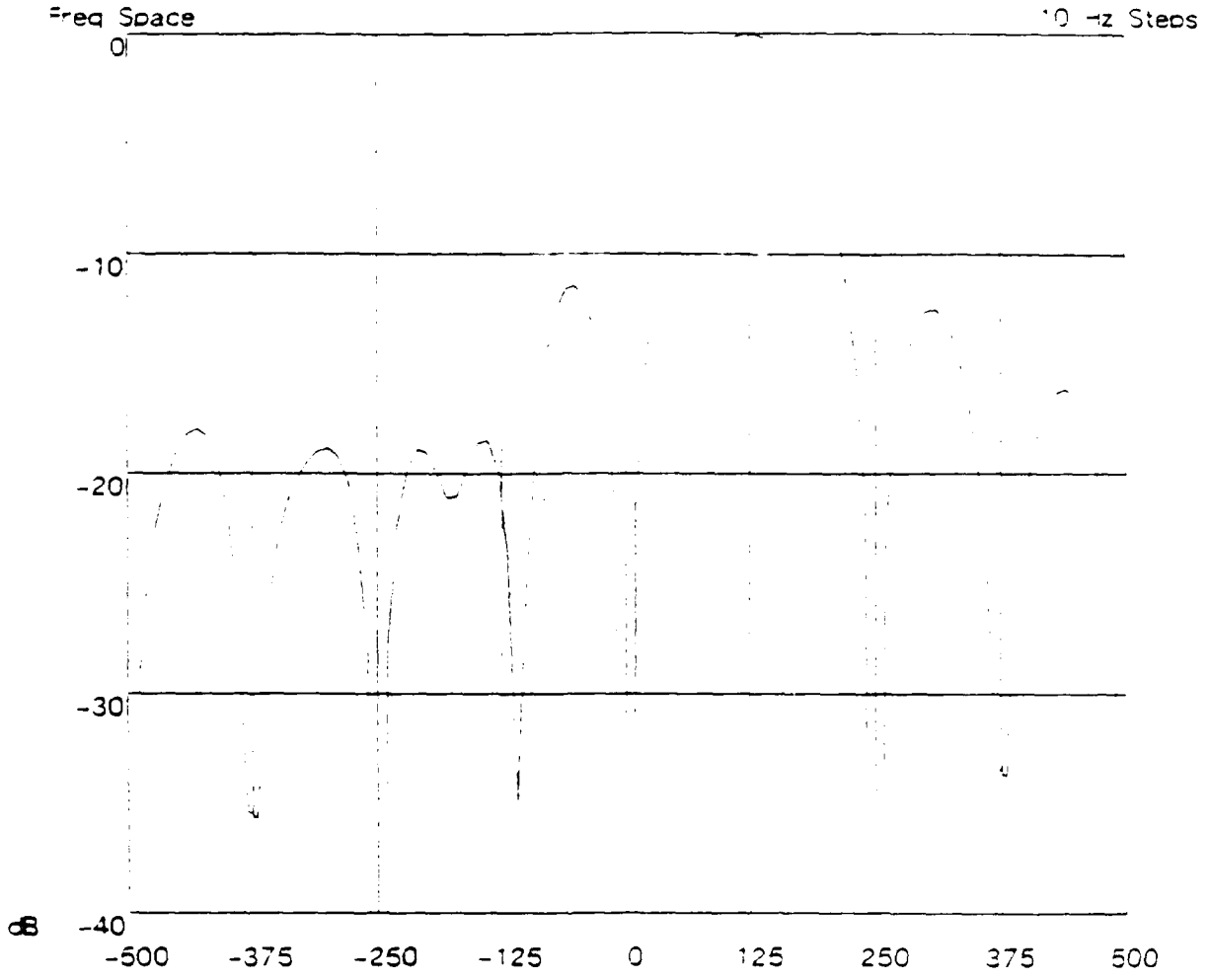

FFT ge=10 Bin1

Figure 6

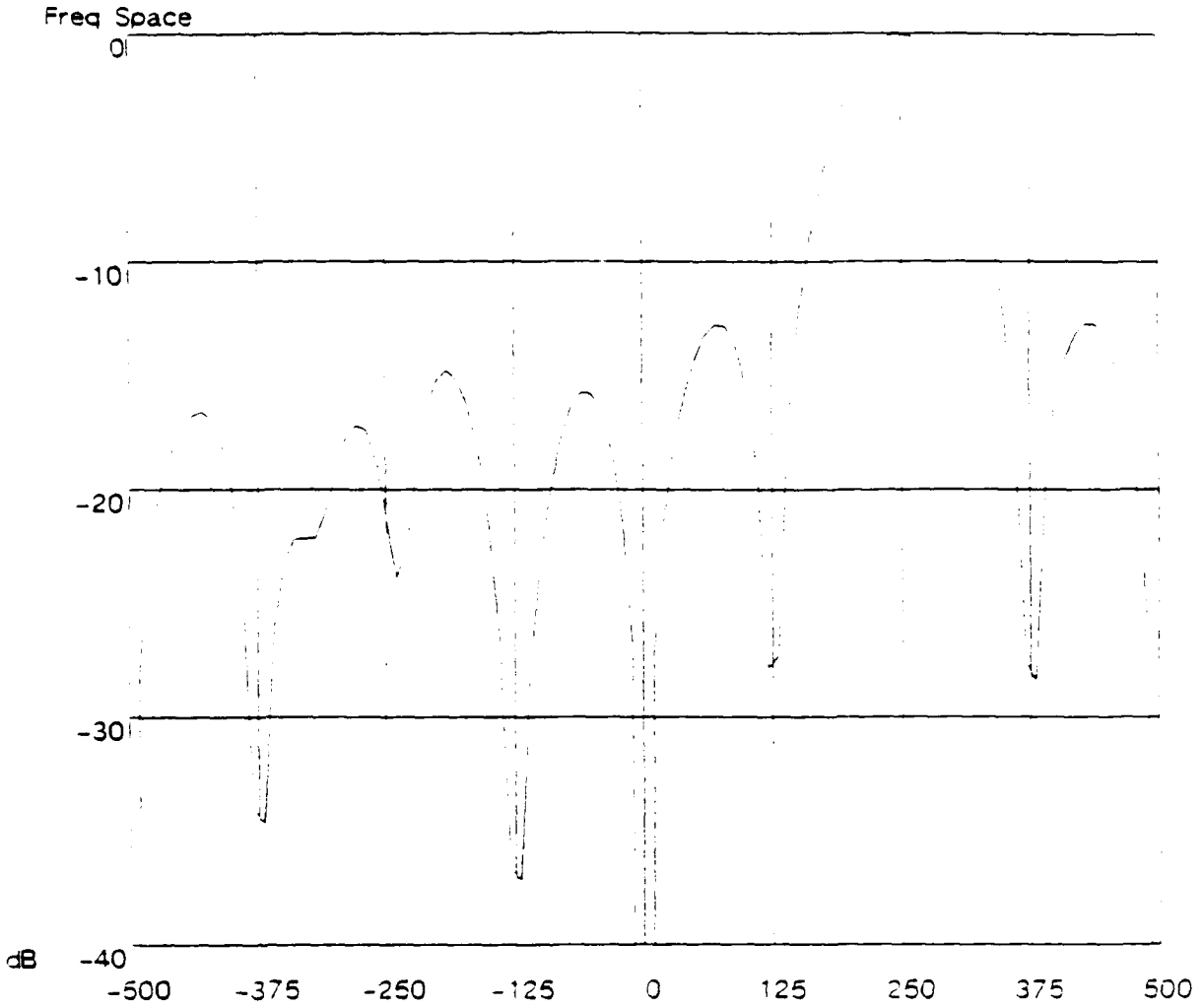

FFT qe=10 Bin 2

Figure 7

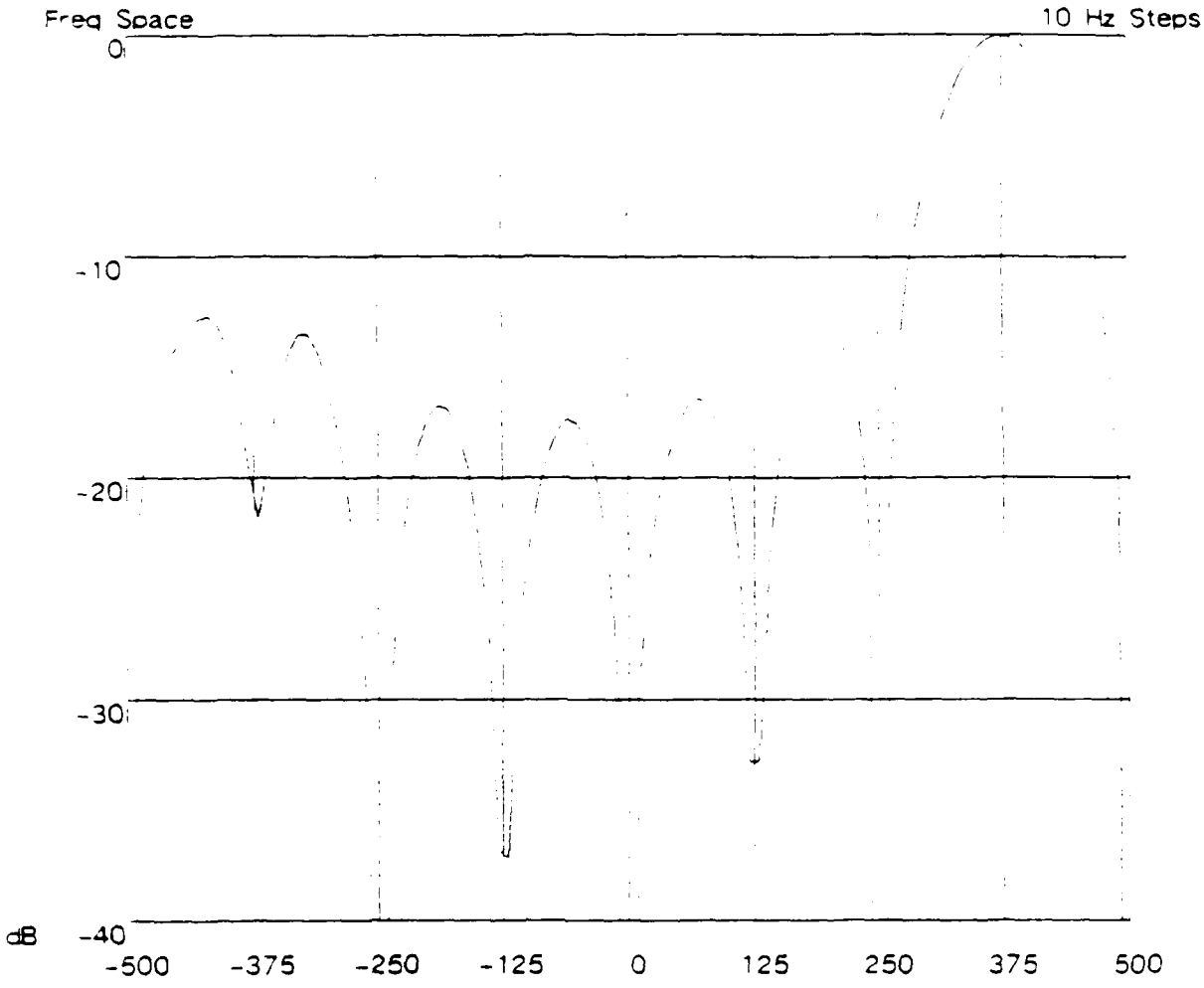

FFT ge=10 Bin3

Figure 8

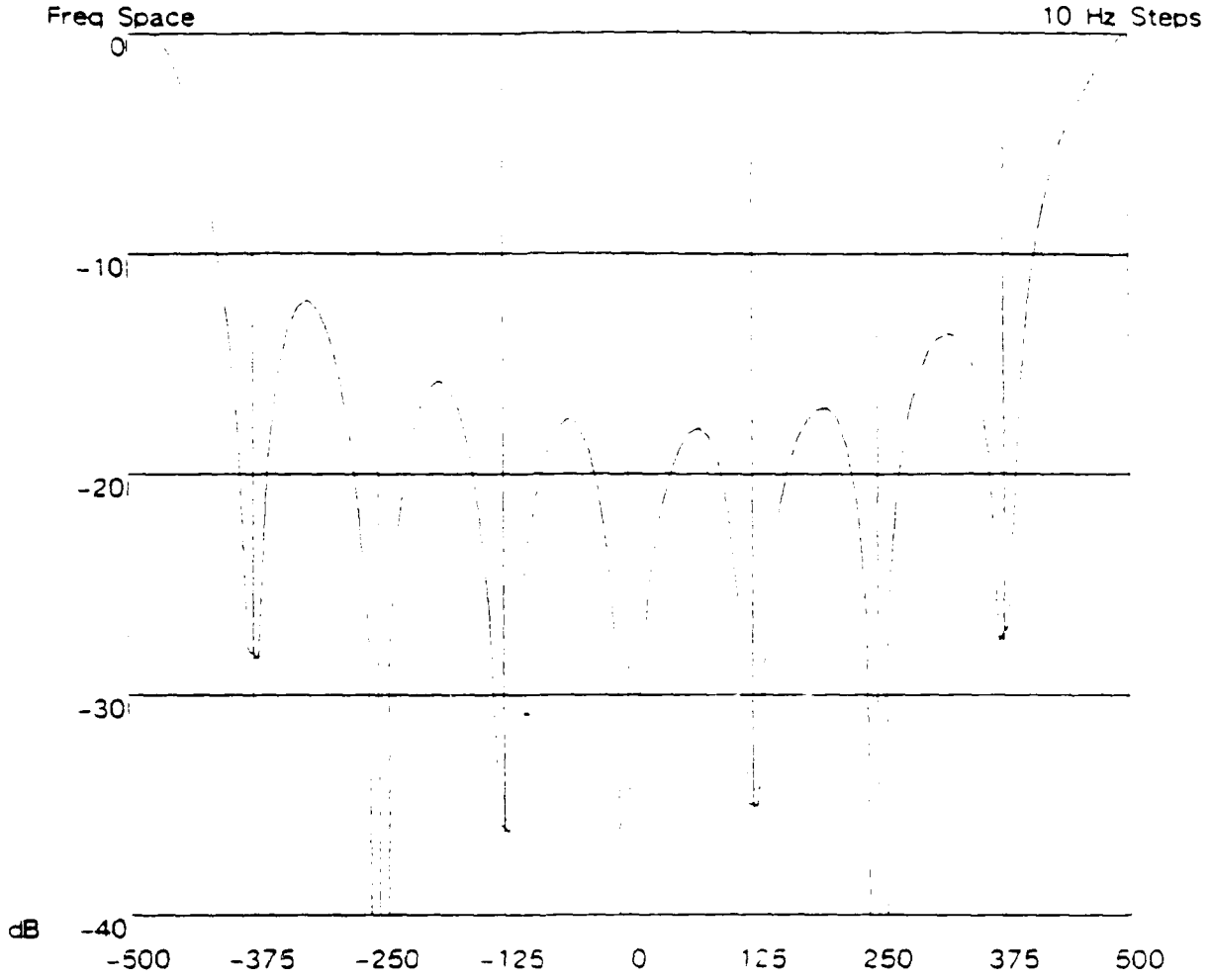

FFT ae=10 Bin4

Figure 9

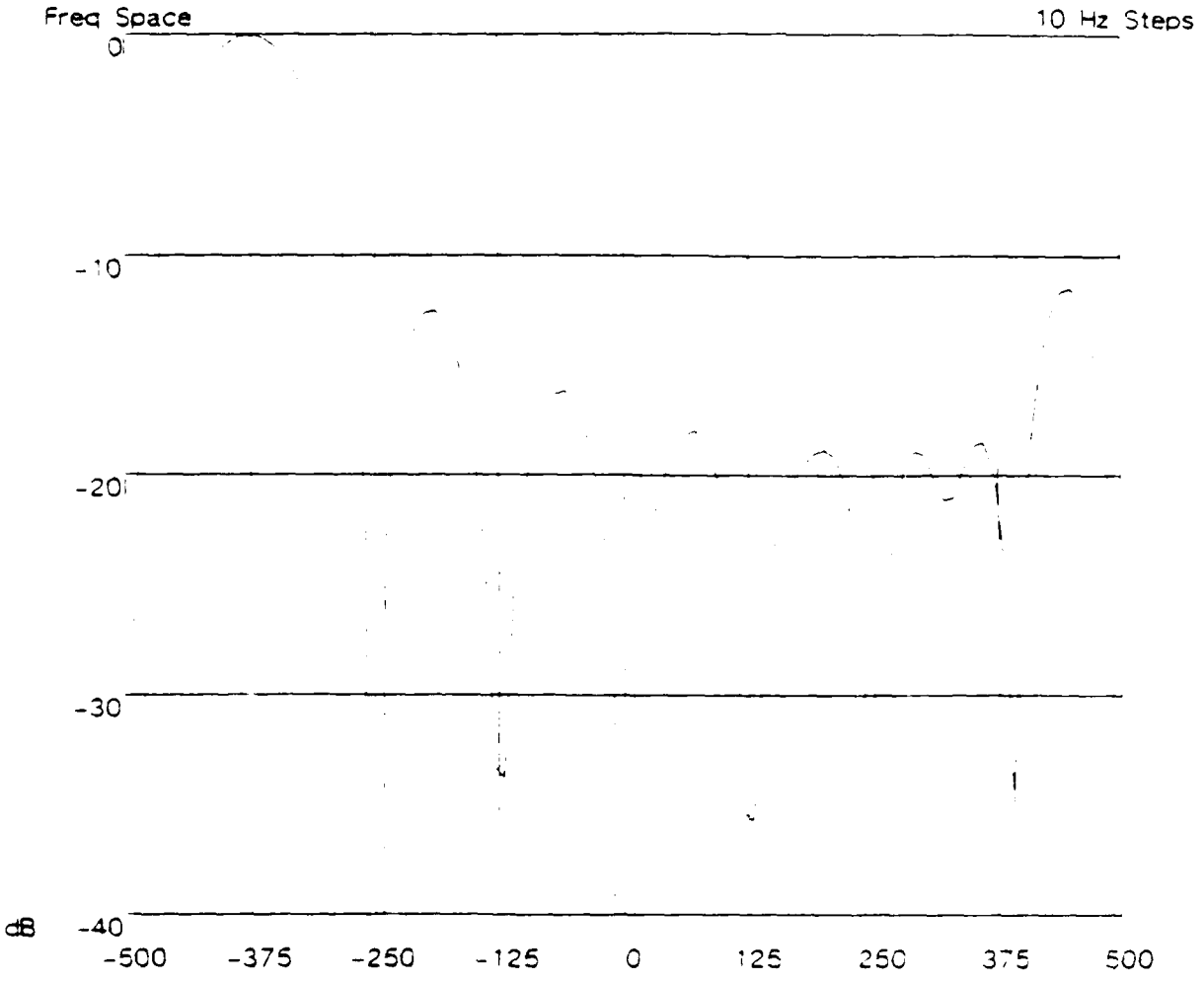

FFT ge=10 Bins

Figure 10

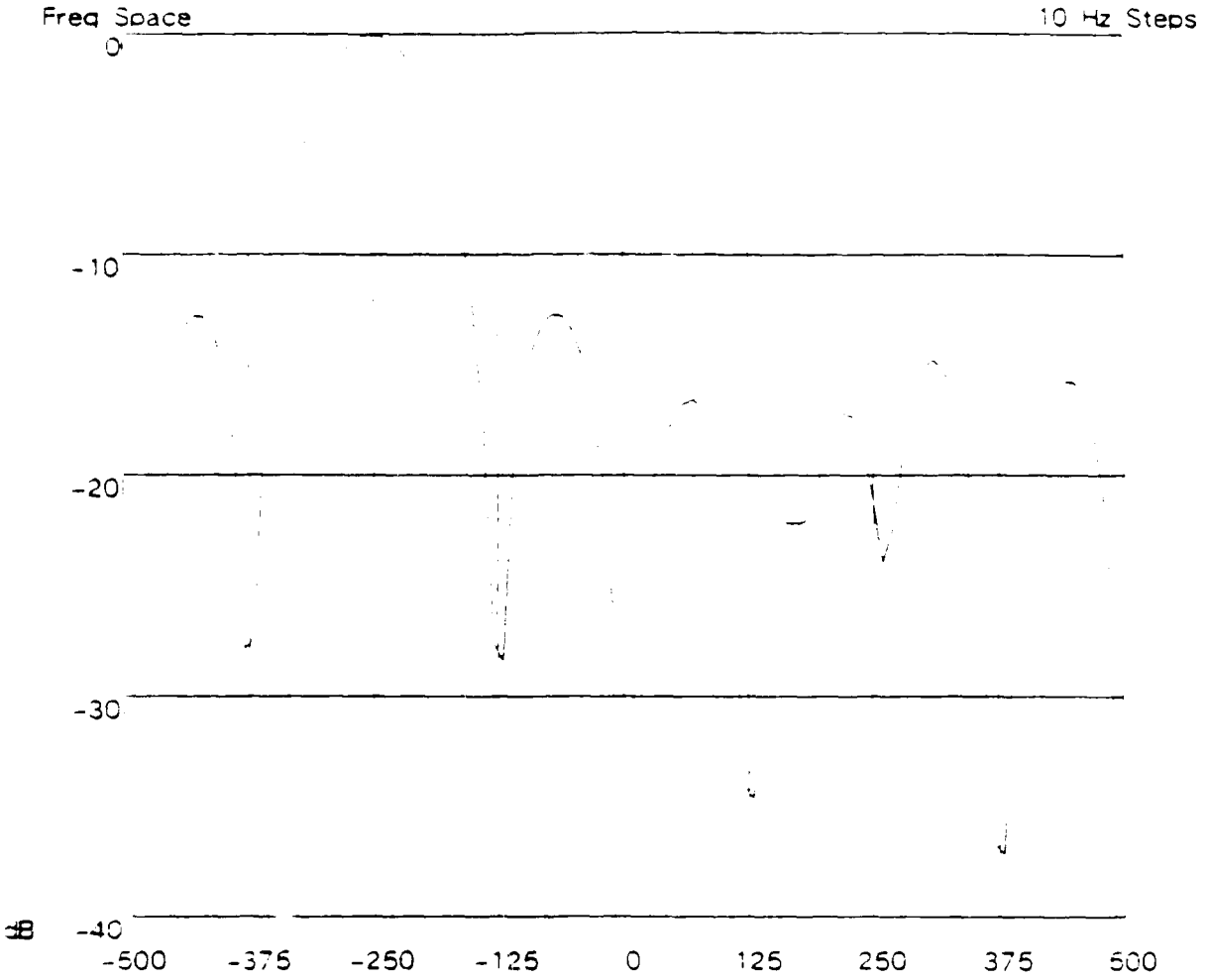

FFT ge=10 Bin6

Figure 11

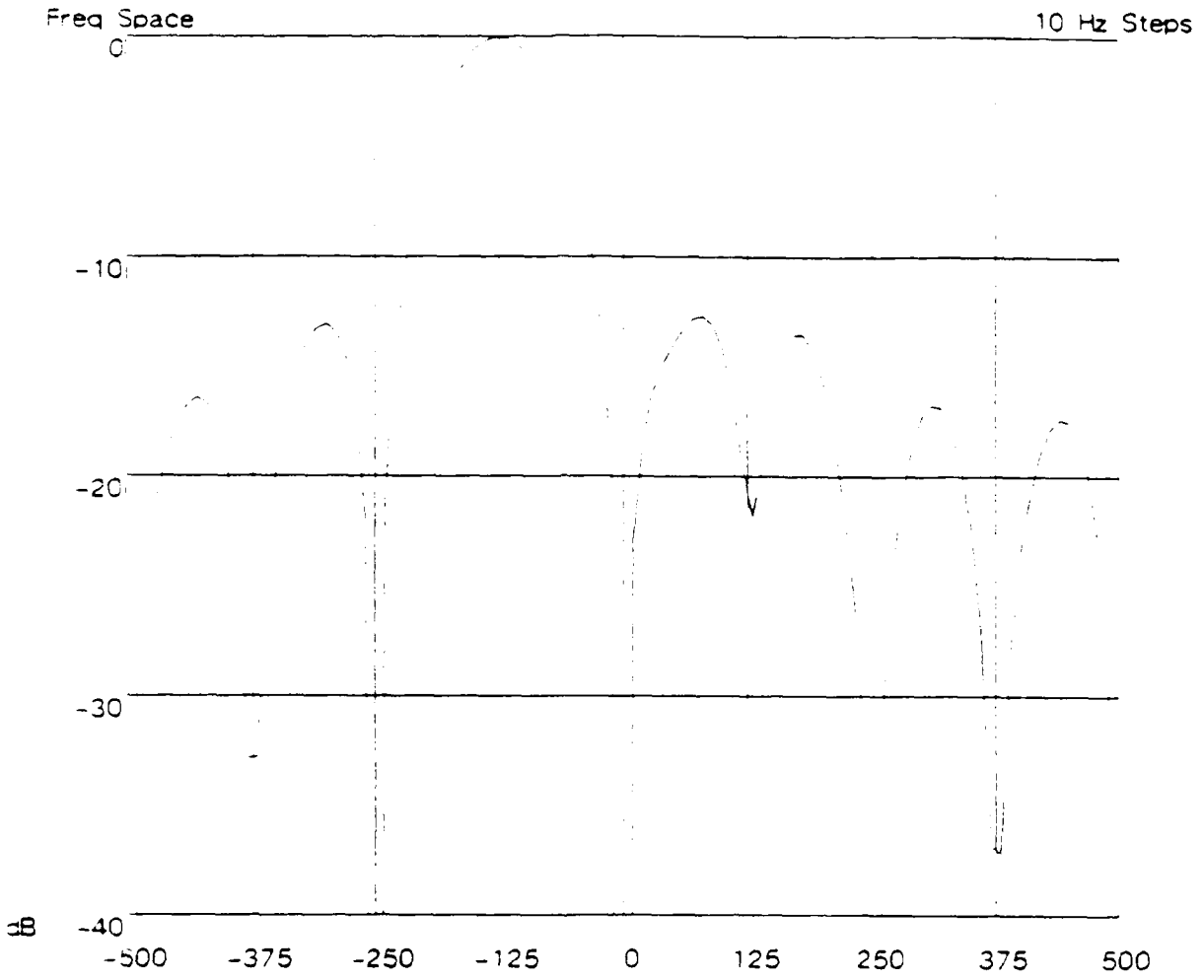

FFT qe=10 Bin7

Figure 12

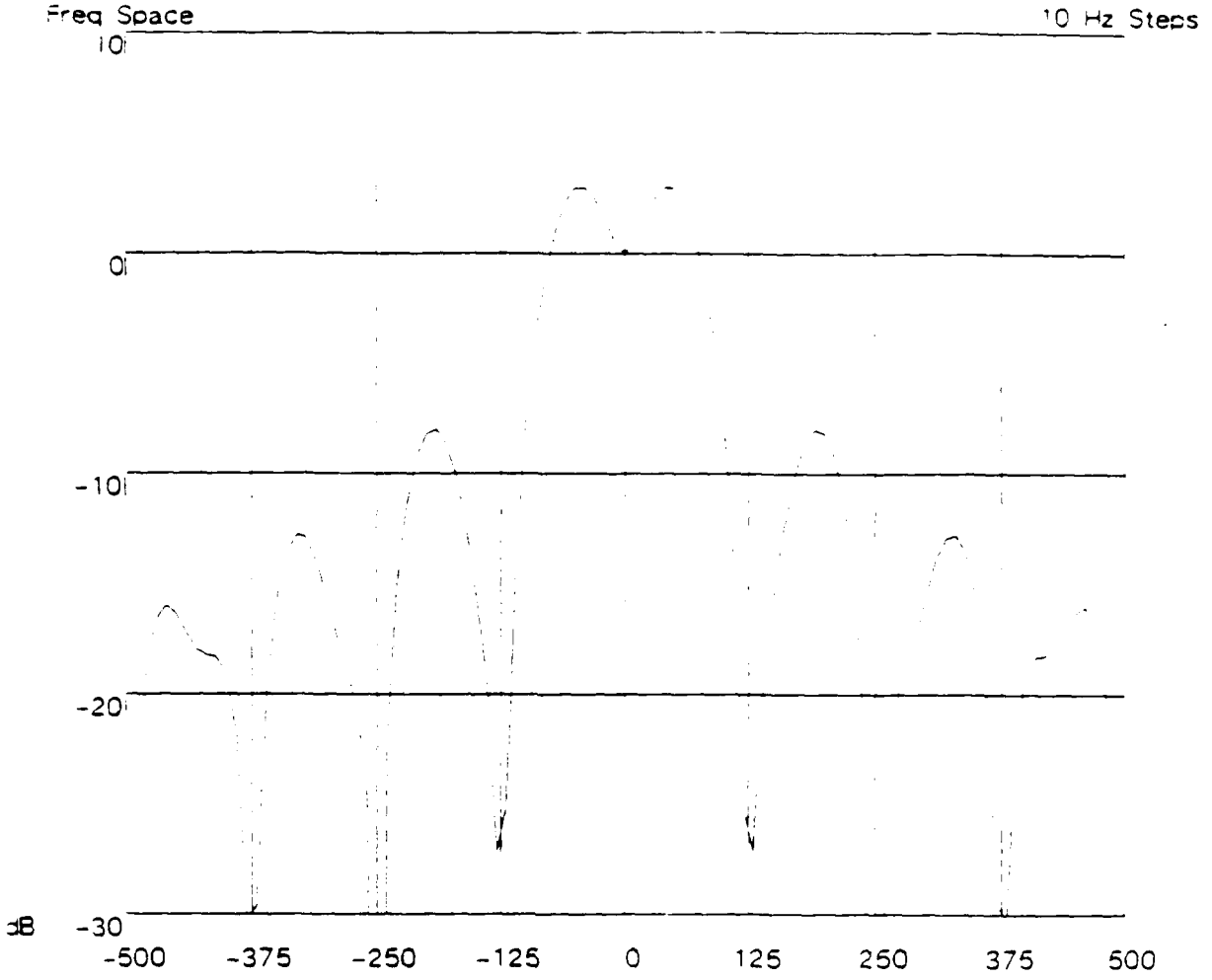

FFT ae=2 Bin 0

Figure 13

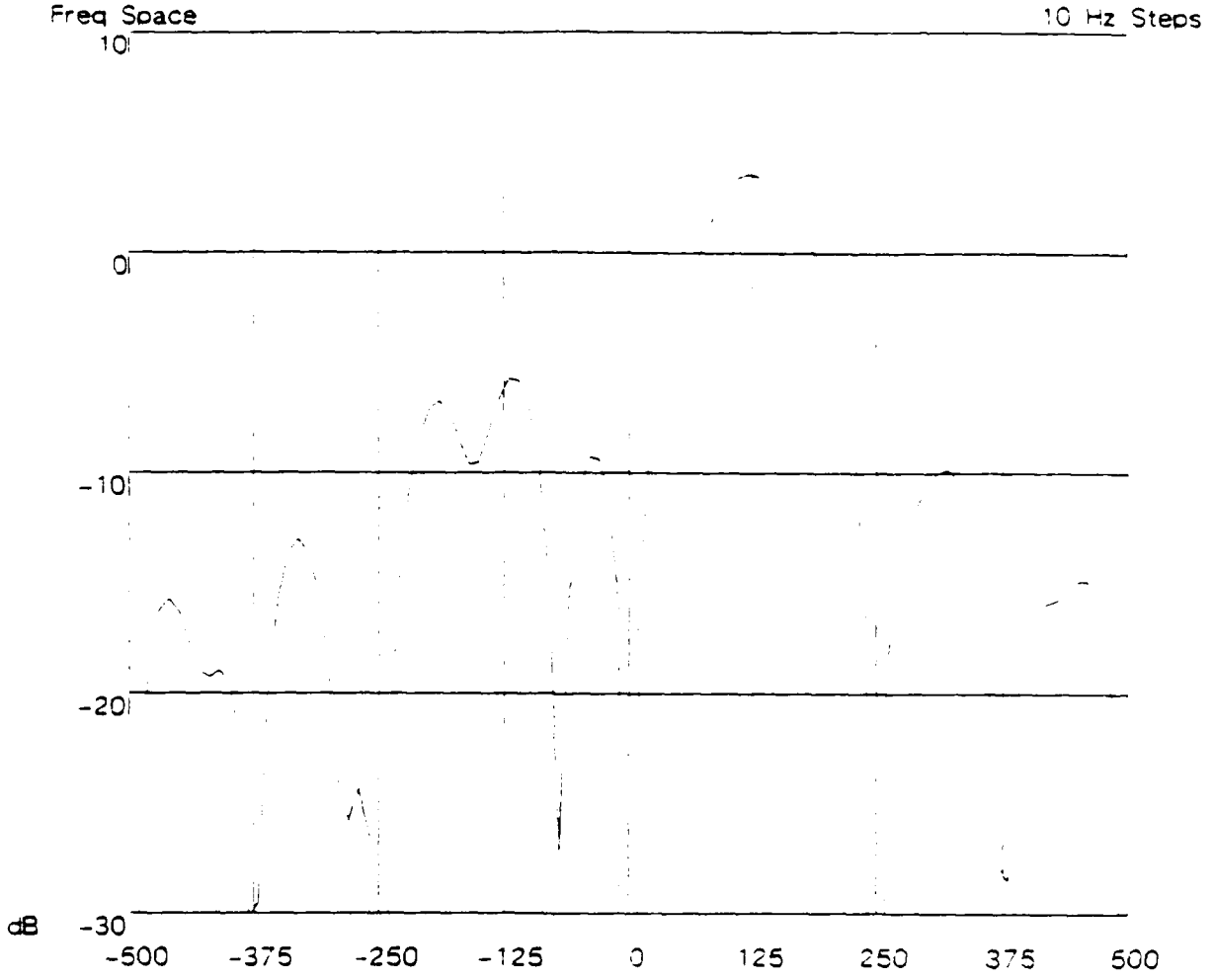

FFT ae=2 Bin 1

Figure 14

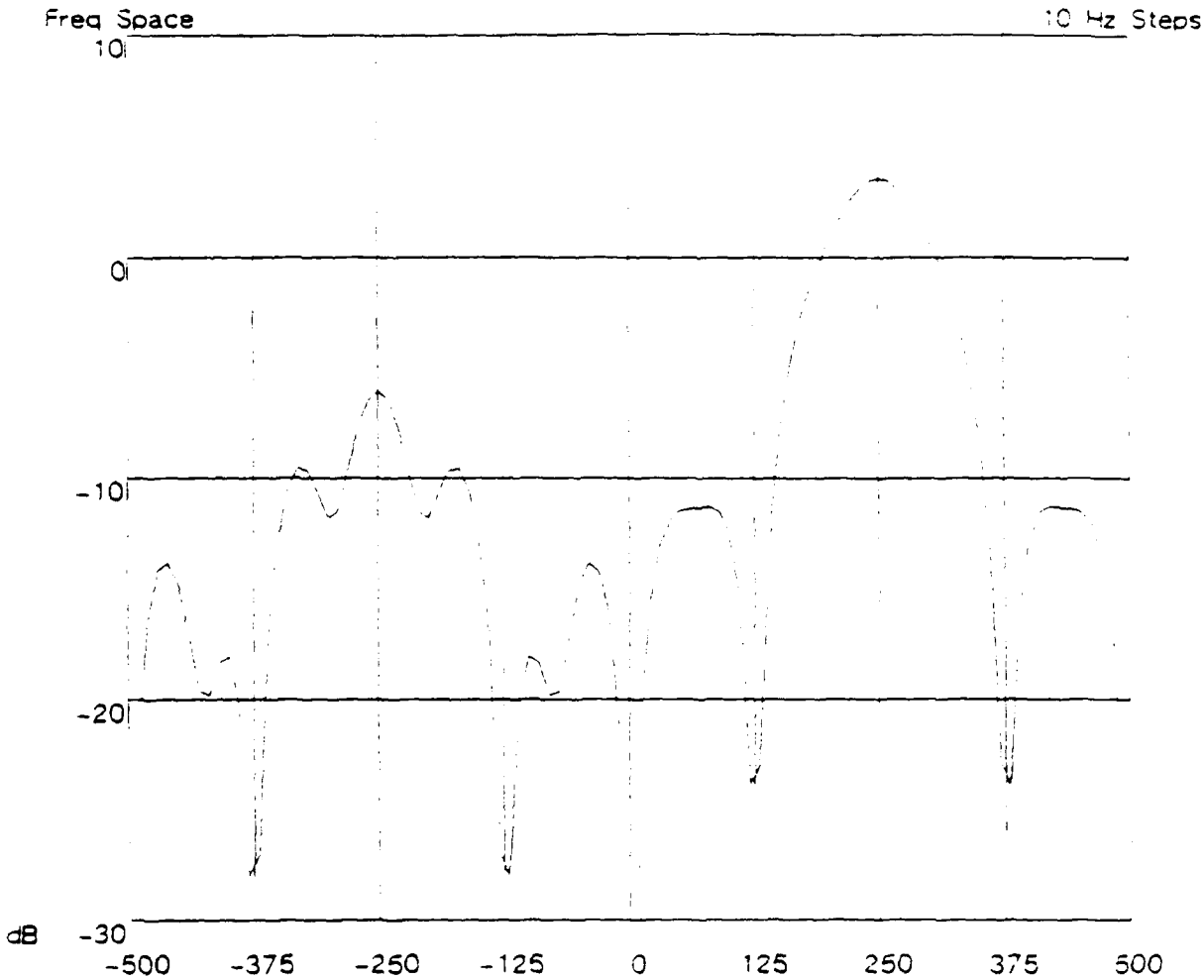

FFT ae=2 Bin 2

Figure 15

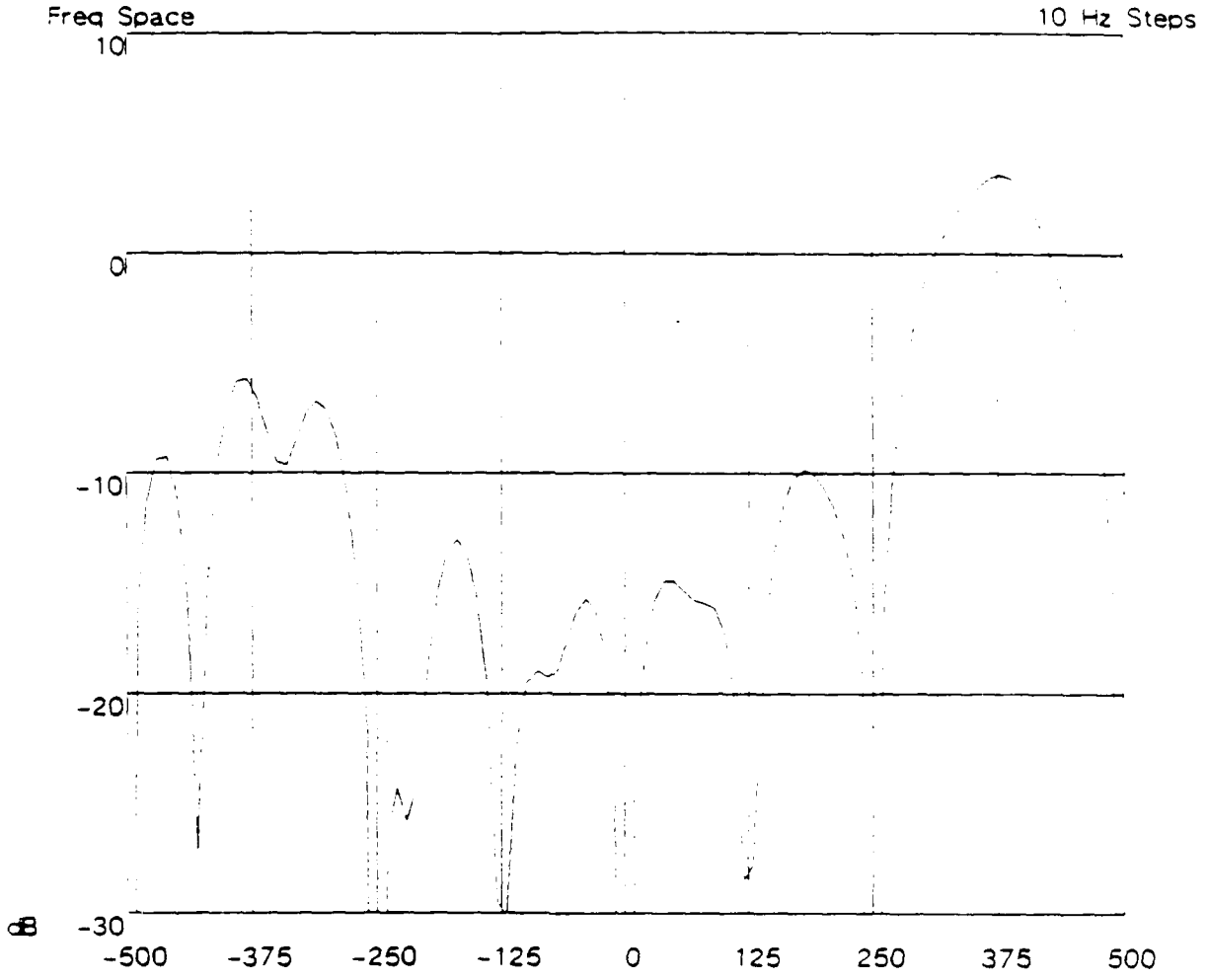

FFT ae=2 Bin 3

Figure 16

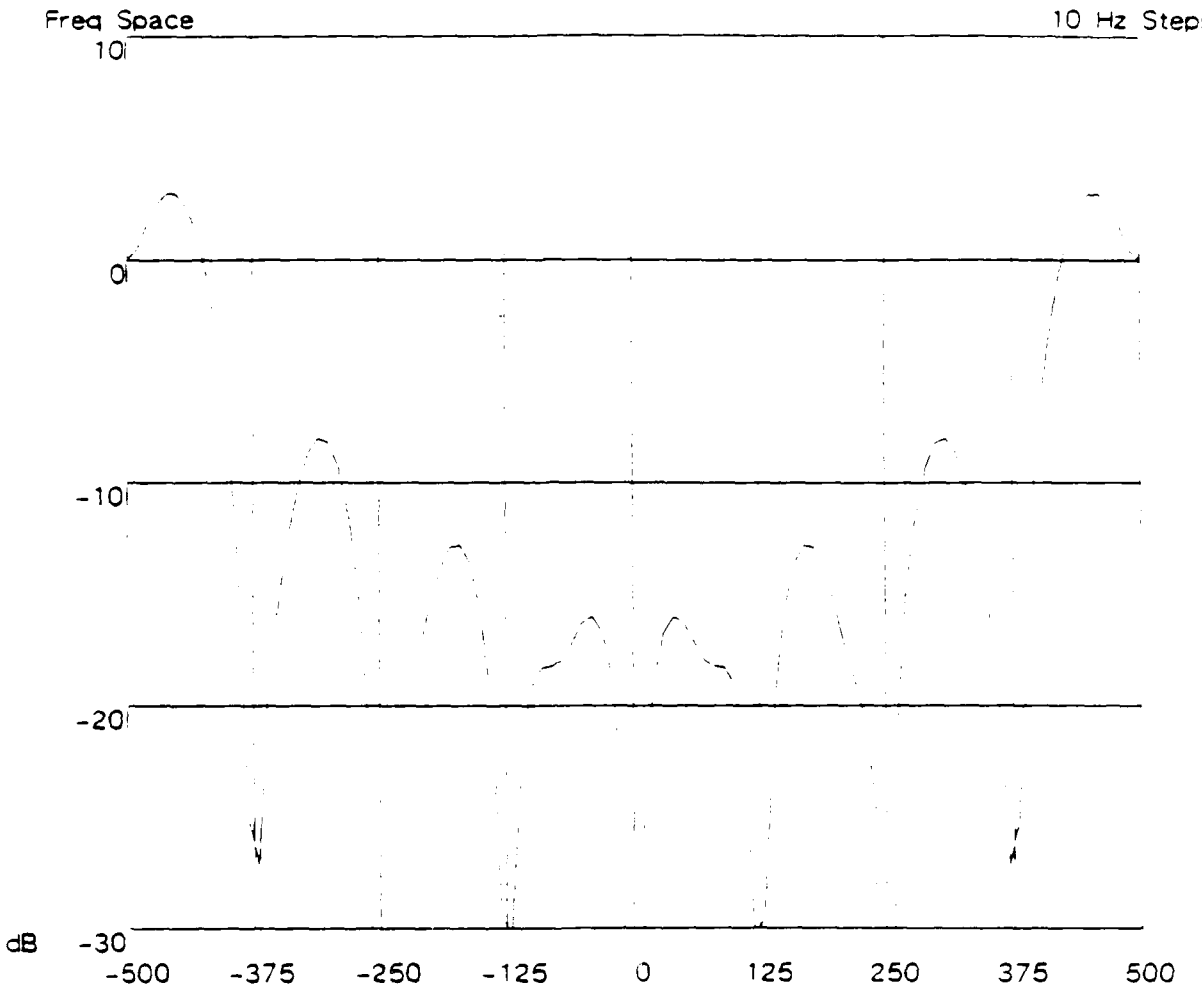

FFT ae=2 Bin 4

Figure 17

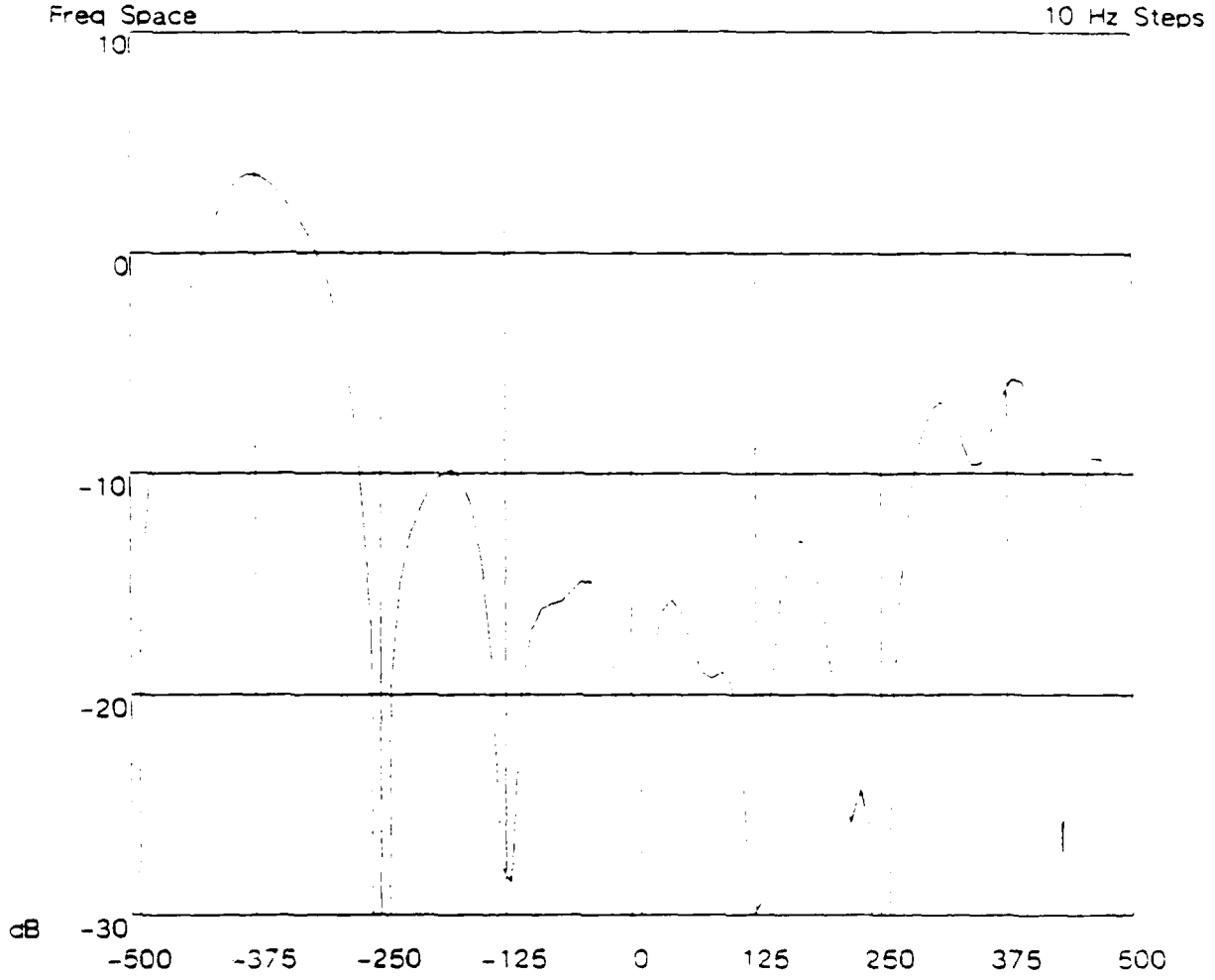

FFT ae=2 Bin 5

Figure 18

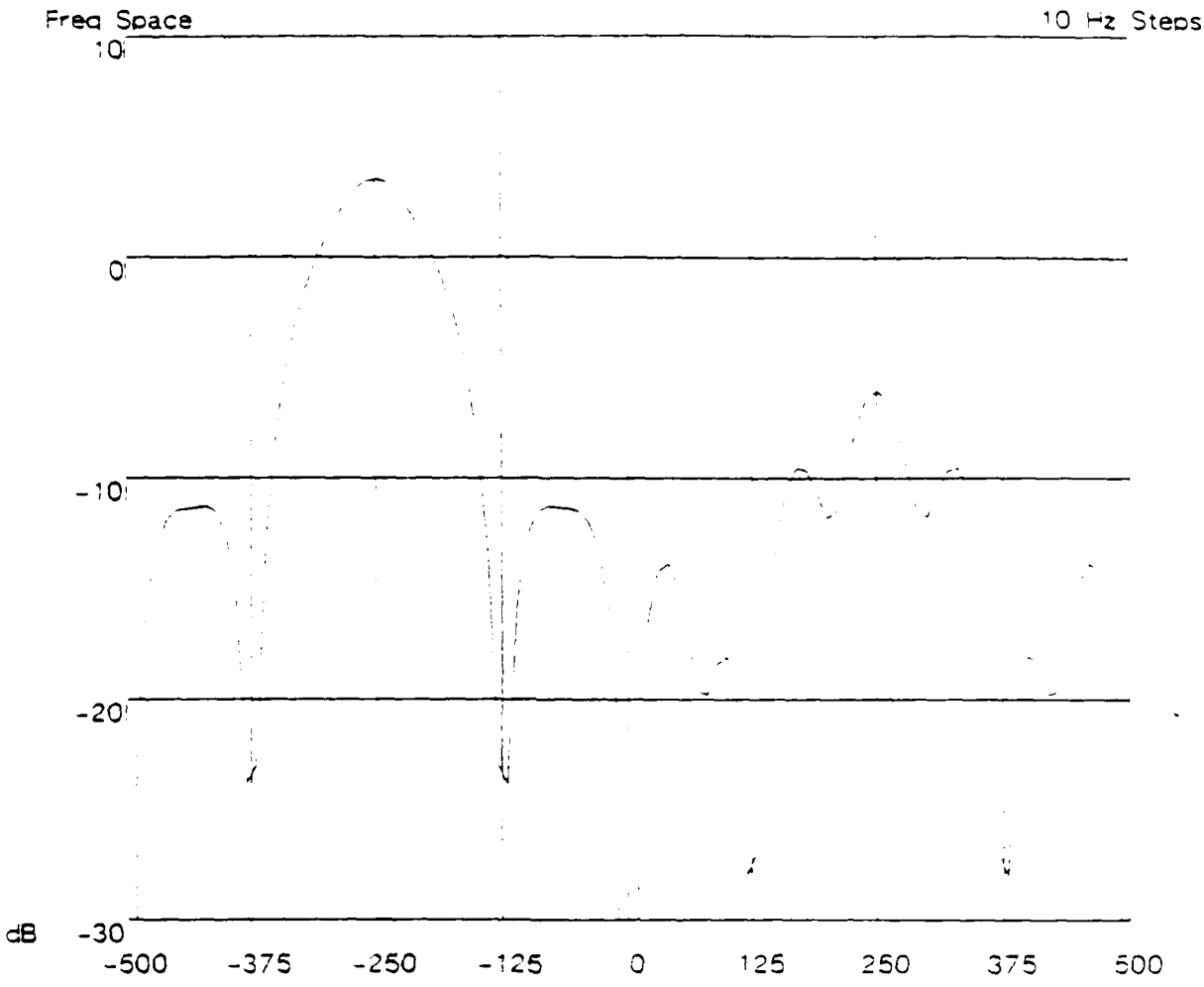

FFT ae=2 Bin 6

Figure 19

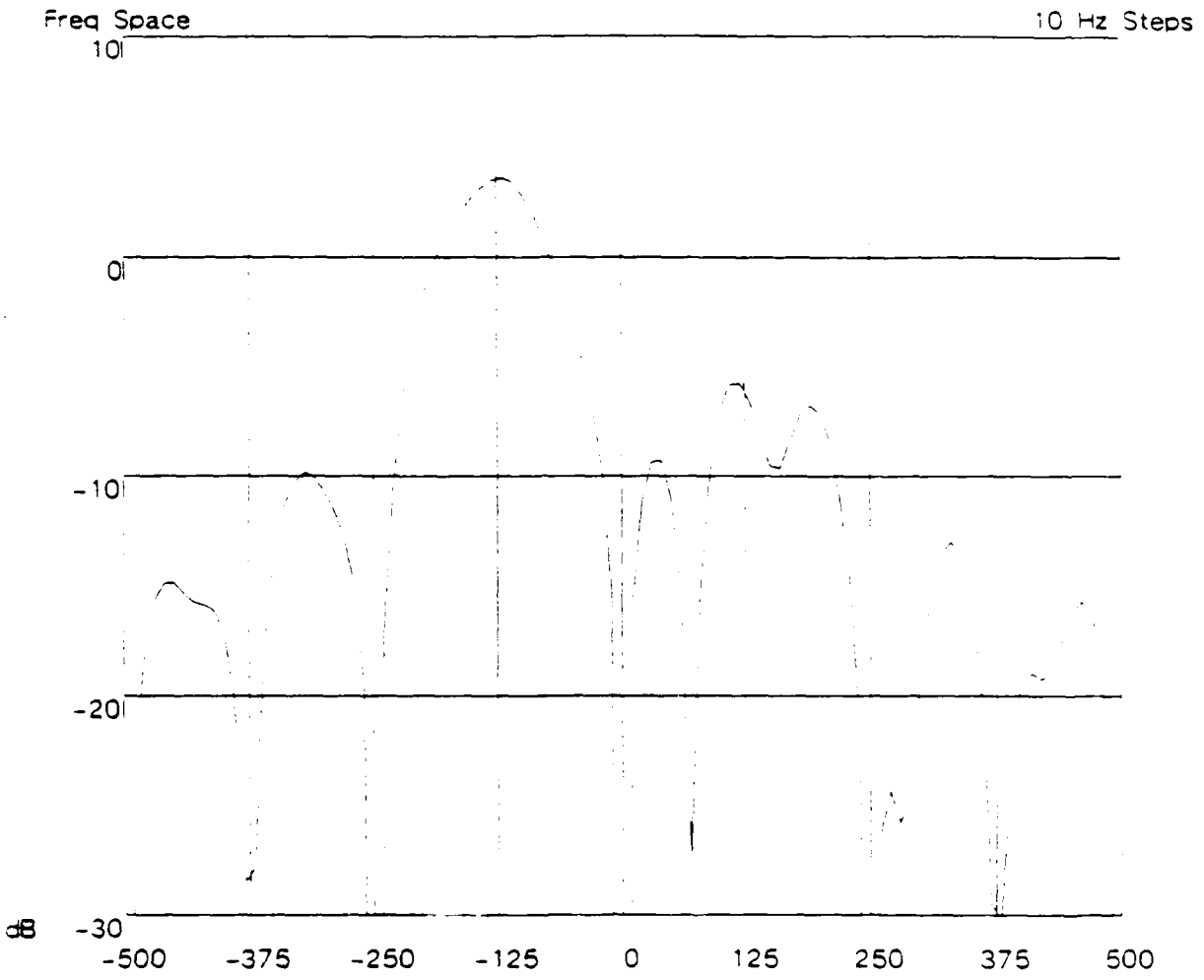

FFT ae=2 Bin 7

Figure 20

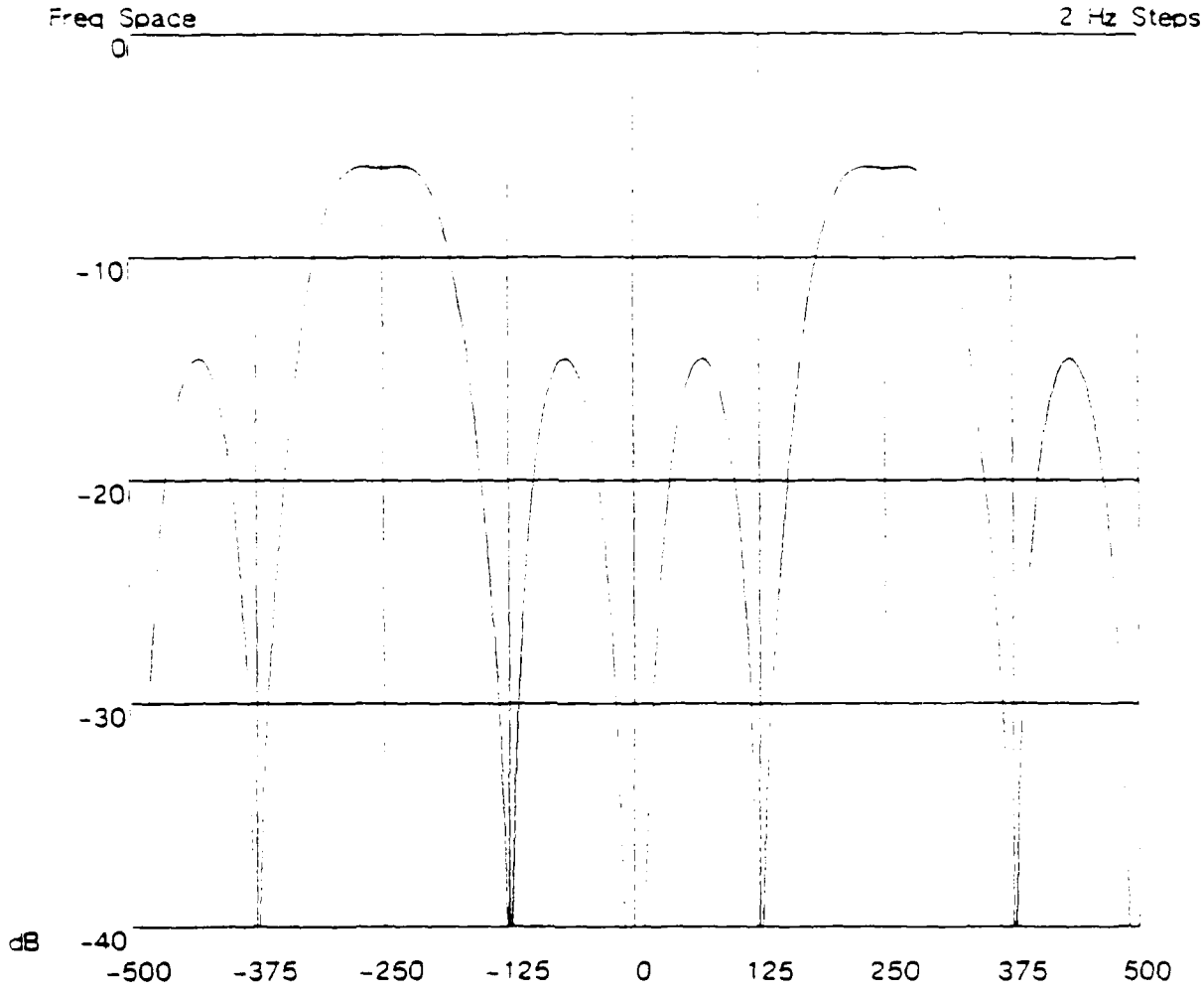

Real FFT Bin 2

Figure 21

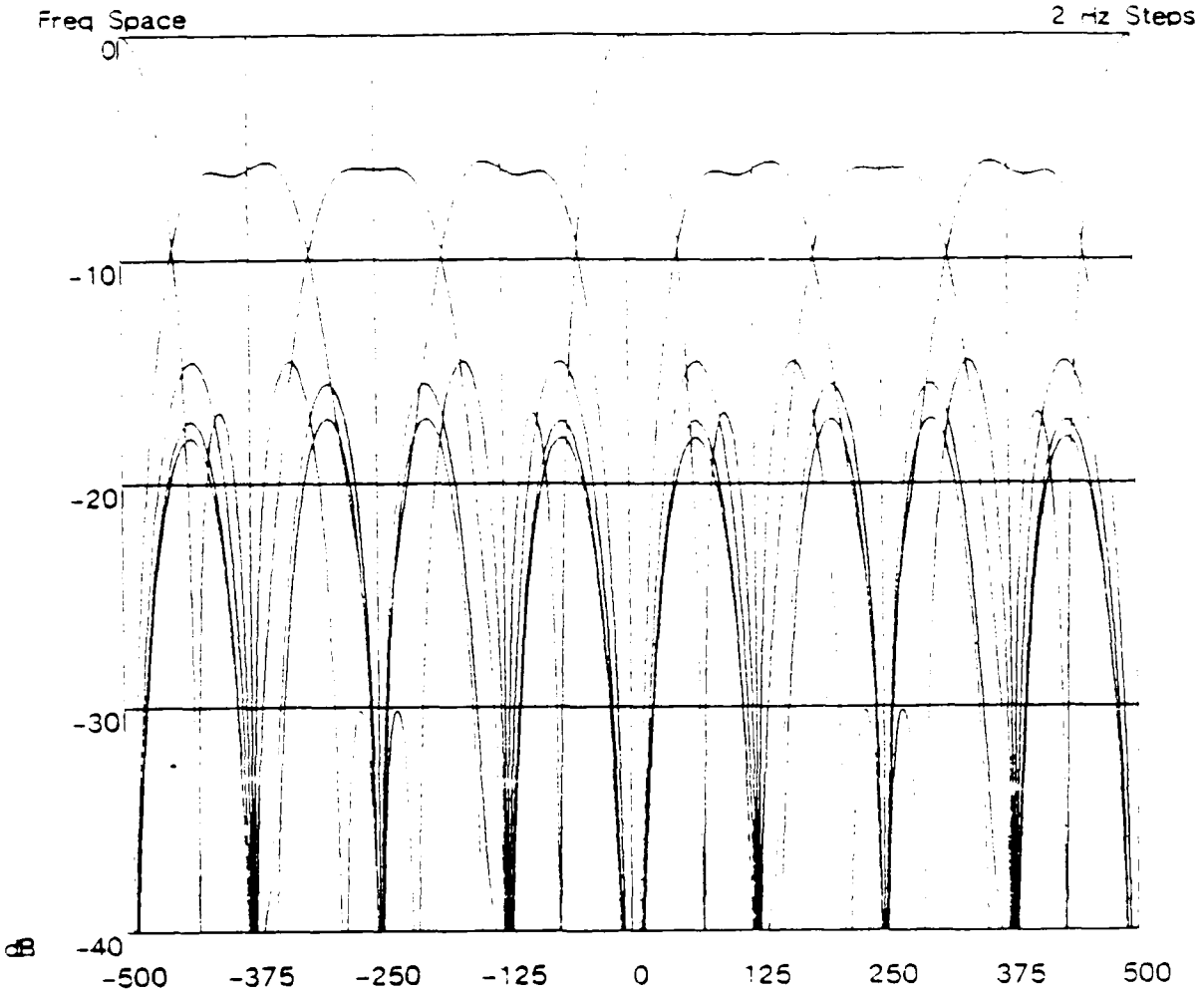

Real FFT

Figure 22

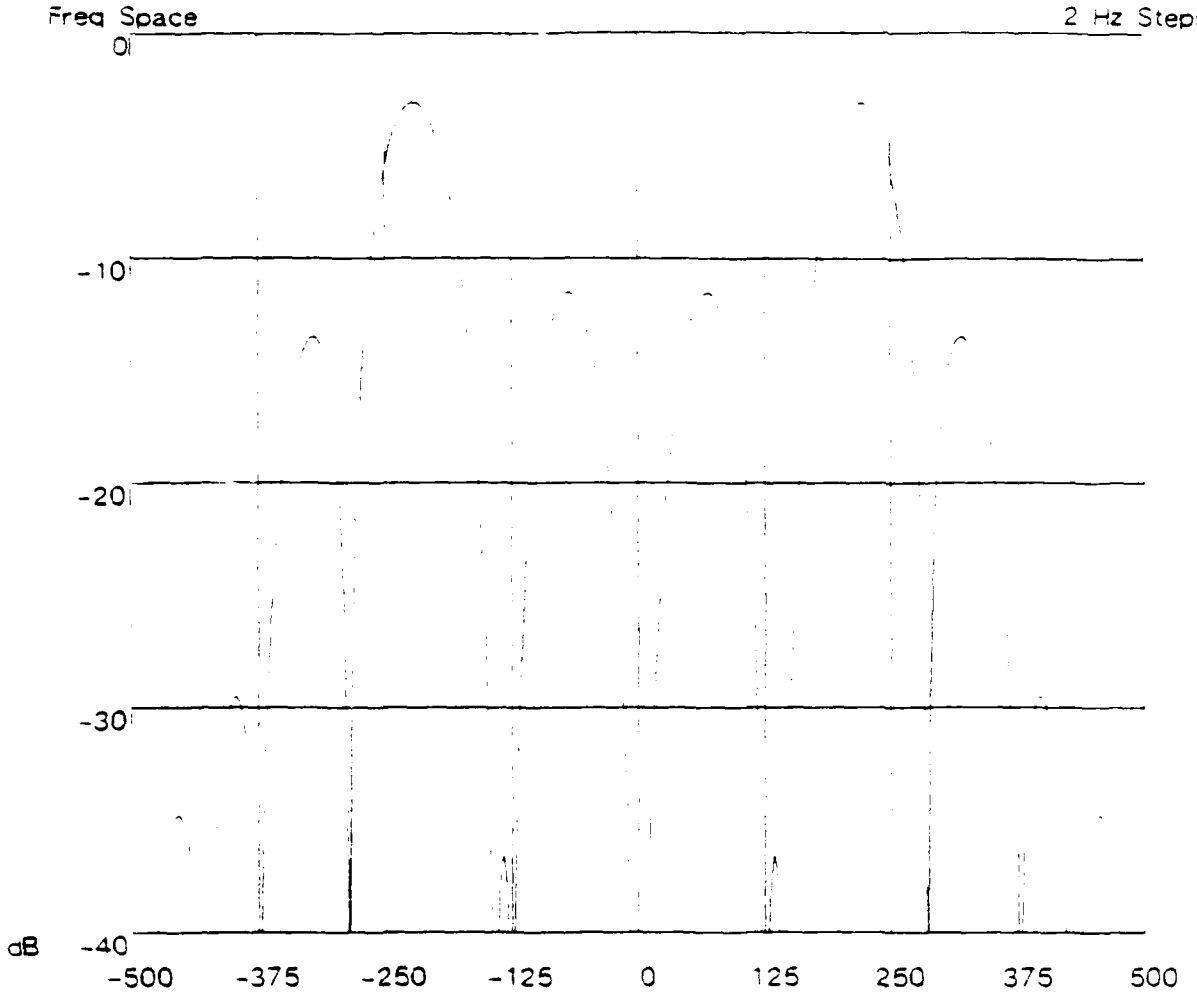

DHT Bin 2

Figure 23

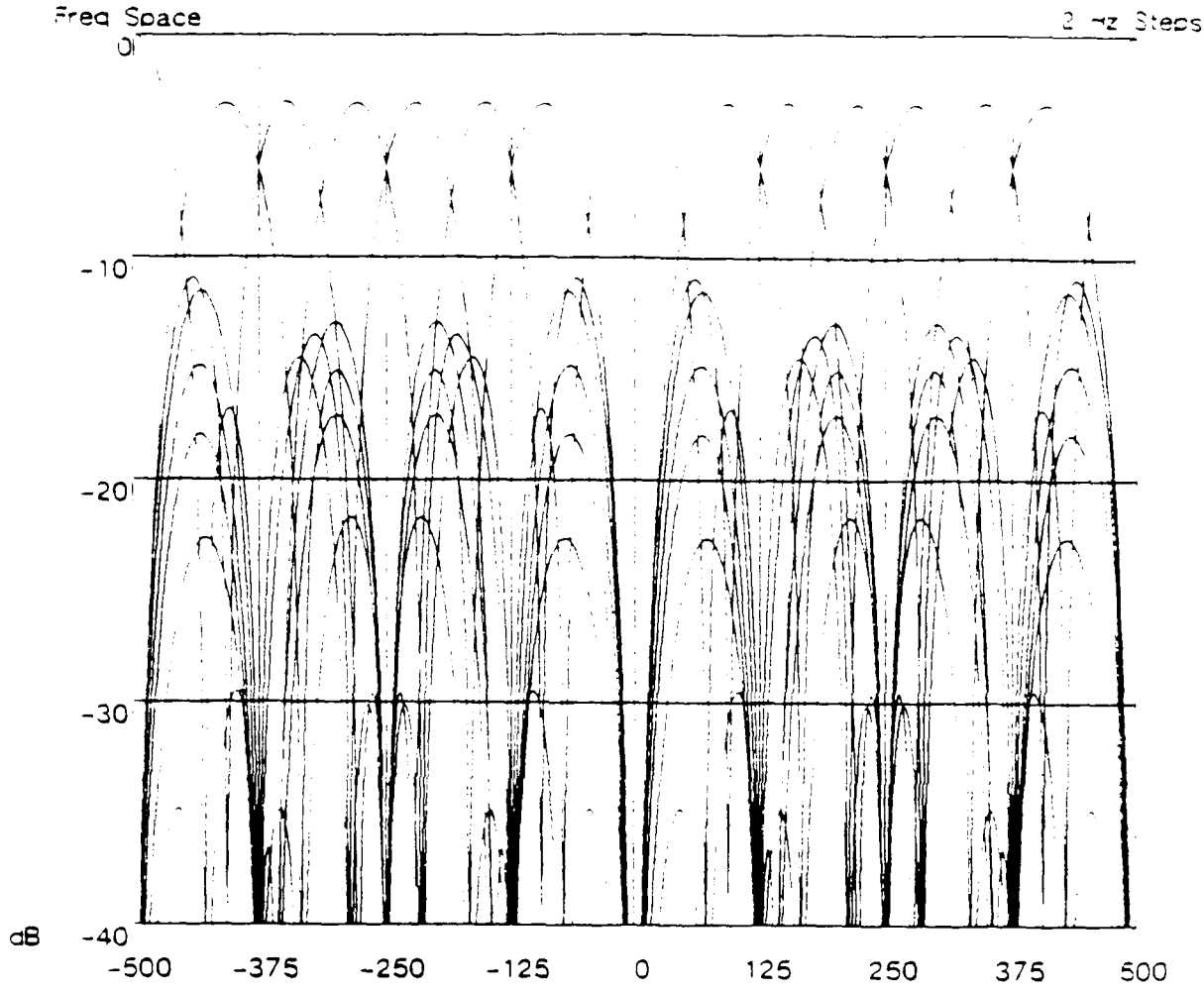

DHT

Figure 24

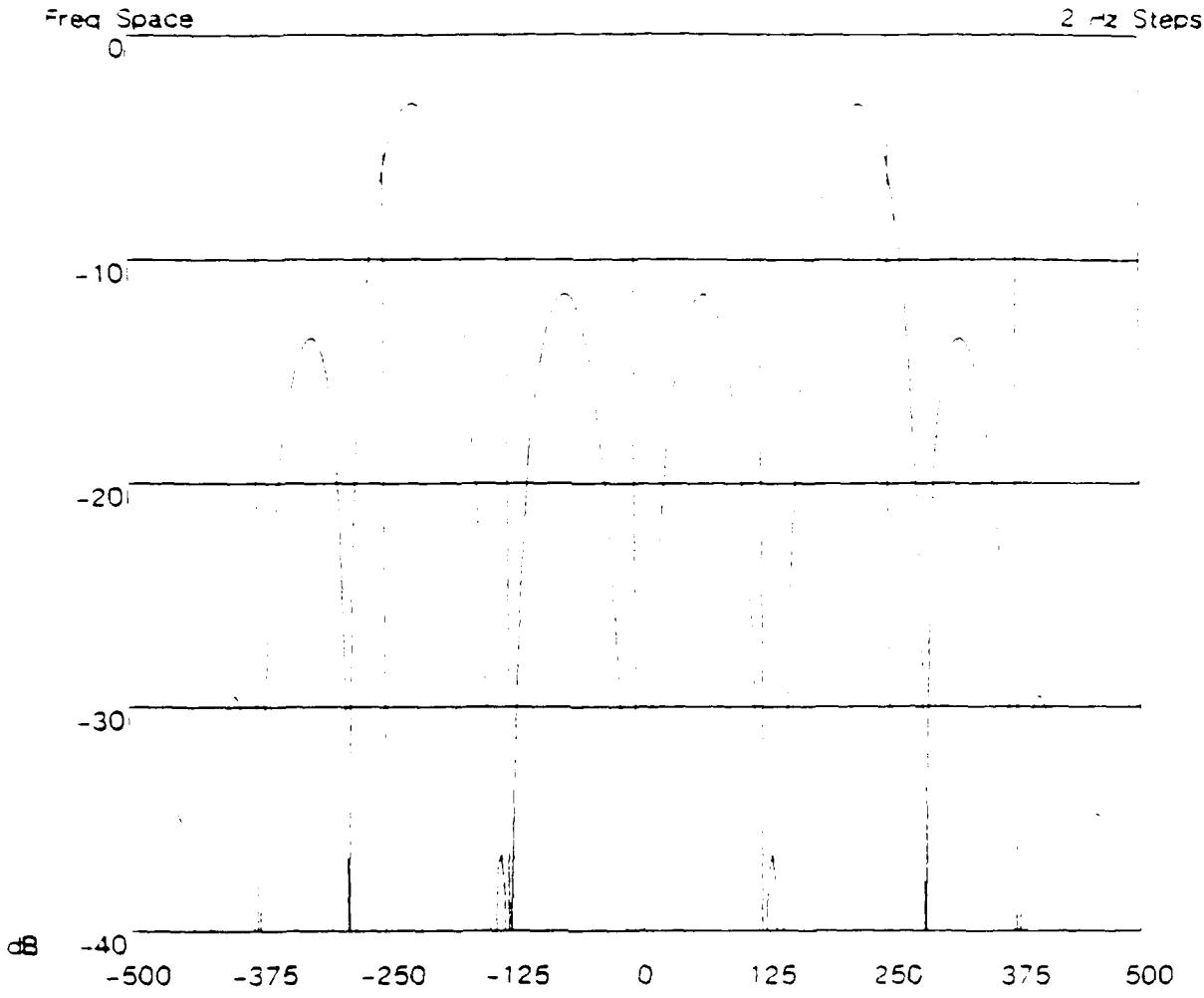

Hadamard Bin 2

Figure 25

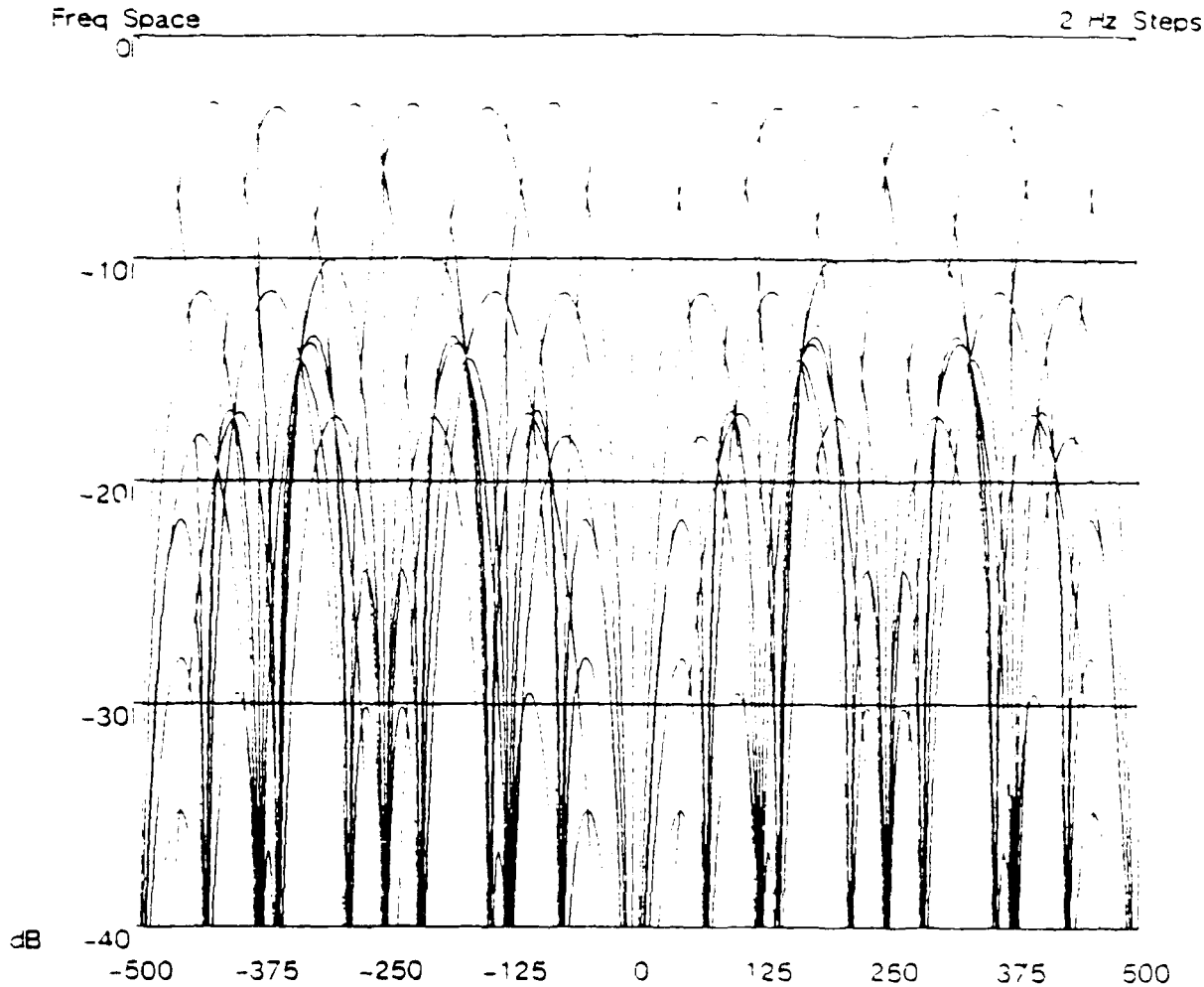

Hadamard

Figure 26

References

1. Harris, F.J., "On the Use of Windows for Harmonic Analysis with the Discrete Fourier Transform," *IEEE Proceedings*, vol. 66, no. 1, pp. 51-83, January 1978.
2. Girgis, A.A. and Ham, F.M., "A Quantitative Study of Pitfalls in the FFT," *IEEE Transactions on Aerospace and Electronics Systems*, vol. AES-16, no. 4, pp. 434-439, July 1980.
3. Sinsky, A.I. and Wang, P.C.P., "Error Analysis of a Quadrature Coherent Detector Processor," *IEEE Transactions on Aerospace and Electronic Systems*, vol. AES-10, no. 6, pp. 880-883, November 1974.
4. Waters, W.M. and Jarrett, B.R., "Tests of Direct-Sampling Coherent Detection with a Laboratory Analog-to-Digital Converter," *IEEE Transaction*, vol. AES-21, May 1985.
5. Churchill, F.E., Ogar, G.W., and Thompson, B.J., "The Correction of I and Q Errors in a Coherent Processor," *IEEE Transactions on Aerospace and Electronic Systems*, vol. AES-17, no. 1, January 1981.
6. Heydemann, P.L.M., "Determination and correction of quadrature fringe measurement errors in interferometers," *Applied Optics*, vol. 20, no. 19, October 1981.
7. Harris, F.J., *Trigonometric Transforms - a unique introduction to the FFT*, Scientific-Atlanta, San Diego, CA, 1981.
8. Storn, R., "Fast Algorithms for the Discrete Hartley Transform," *AEU*, 1986.
9. Lee, M.H. and Kaveh, M., "Fast Hadamard Transform Based on a Simple Matrix Factorization," *IEEE Transactions on Acoustics, Speech, and Signal Processing*, vol. ASSP-34, no. 6, December 1986.
10. Bracewell, R.N., *The Fourier Transform and its Applications*, pp. 104-107, McGraw-Hill, 1986.

Appendix

The DFT of a signal with a phase quadrature error is derived as follows

$$F_p(\theta) = N^{-1}\sum_{n=0}^{N-1}[\cos(n\theta_0) + j\sin(n\theta_0 - T)]\, e^{-jn\theta}$$

$$= \frac{1}{N}\sum_{n=0}^{N-1}\cos(n\theta_0)e^{-jn\theta} + \frac{1}{N}\sum_{n=0}^{N-1} j\sin(n\theta_0 - T)e^{-jn\theta}$$

Shift Theorem : $f(\tau - T) \;\langle\text{---}\rangle\; e^{-j\frac{2\pi\nu T}{N}} F(\nu)$

By using the shift theorem the following can be shown :

$$\frac{1}{N}\sum_{n=0}^{N-1} j\sin(n\theta_0 - T)e^{-jn\theta} = \frac{1}{N}e^{-j\theta T}\sum_{n=0}^{N-1} j\left[\frac{e^{jn\theta_0}}{j2} - \frac{e^{-jn\theta_0}}{j2}\right]e^{-jn\theta}$$

$$= \frac{1}{2N}e^{-j\theta T}\sum_{n=0}^{N-1}\left[e^{jn\theta_0} - e^{-jn\theta_0}\right]e^{-jn\theta} = \frac{1}{N}e^{-j\theta T}\sum_{n=0}^{N-1}\left[\frac{1}{2}e^{-jn(\theta-\theta_0)} - \frac{1}{2}e^{-jn(\theta+\theta_0)}\right]$$

$$= e^{-j\theta T}\left\{\frac{1}{2N}e^{-j\left[\frac{N-1}{2}\right](\theta-\theta_0)}\left[\frac{\sin\left[\frac{N}{2}(\theta-\theta_0)\right]}{\sin\left[\frac{1}{2}(\theta-\theta_0)\right]}\right] - \frac{1}{2N}e^{-j\left[\frac{N-1}{2}\right](\theta+\theta_0)}\left[\frac{\sin\left[\frac{N}{2}(\theta+\theta_0)\right]}{\sin\left[\frac{1}{2}(\theta+\theta_0)\right]}\right]\right\}$$

$$F_p(\theta) = \frac{1}{2N}e^{-j\left[\frac{N-1}{2}\right](\theta-\theta_0)}\left[\frac{\sin\left[\frac{N}{2}(\theta-\theta_0)\right]}{\sin\left[\frac{1}{2}(\theta-\theta_0)\right]}\right] + e^{-j\theta T}\left\{\frac{1}{2N}e^{-j\left[\frac{N-1}{2}\right](\theta-\theta_0)}\left[\frac{\sin\left[\frac{N}{2}(\theta-\theta_0)\right]}{\sin\left[\frac{1}{2}(\theta-\theta_0)\right]}\right]\right\} +$$

$$\frac{1}{2N}e^{-j\left[\frac{N-1}{2}\right](\theta+\theta_0)}\left[\frac{\sin\left[\frac{N}{2}(\theta+\theta_0)\right]}{\sin\left[\frac{1}{2}(\theta+\theta_0)\right]}\right] - e^{-j\theta T}\left\{\frac{1}{2N}e^{-j\left[\frac{N-1}{2}\right](\theta+\theta_0)}\left[\frac{\sin\left[\frac{N}{2}(\theta+\theta_0)\right]}{\sin\left[\frac{1}{2}(\theta+\theta_0)\right]}\right]\right\}$$

The DFT of a signal with an amplitude quadrature error is derived as follows

$$F_a(\theta) = N^{-1}\sum_{n=0}^{N-1}[\cos(n\theta_0) + j(1+\epsilon)\sin(n\theta_0)]e^{-jn\theta}$$

$$= \frac{1}{N}\sum_{n=0}^{N-1}\cos(n\theta_0)e^{-jn\theta} + \frac{1}{N}\sum_{n=0}^{N-1}j(1+\epsilon)\sin(n\theta_0)e^{-jn\theta}$$

$$\frac{1}{N}\sum_{n=0}^{N-1}j(1+\epsilon)\sin(n\theta_0)e^{-jn\theta} = \frac{1}{N}\sum_{n=0}^{N-1}j(1+\epsilon)\left[\frac{e^{jn\theta_0}-e^{-jn\theta_0}}{j2}\right]e^{-jn\theta}$$

$$= \frac{1}{N}\sum_{n=0}^{N-1}\frac{(1+\epsilon)}{2}\left[e^{jn\theta_0}-e^{-jn\theta_0}\right]e^{-jn\theta} = \frac{1}{N}\sum_{n=0}^{N-1}\left[\frac{(1+\epsilon)}{2}e^{-jn(\theta-\theta_0)} - \frac{(1+\epsilon)}{2}e^{-jn(\theta+\theta_0)}\right]$$

$$= \frac{(1+\epsilon)}{2N}e^{-j\left[\frac{N-1}{2}\right](\theta-\theta_0)}\left[\frac{\left|\sin\left[\frac{N}{2}(\theta-\theta_0)\right]\right|}{\left|\sin\left[\frac{1}{2}(\theta-\theta_0)\right]\right|}\right] - \frac{(1+\epsilon)}{2N}e^{-j\left[\frac{N-1}{2}\right](\theta+\theta_0)}\left[\frac{\left|\sin\left[\frac{N}{2}(\theta+\theta_0)\right]\right|}{\left|\sin\left[\frac{1}{2}(\theta+\theta_0)\right]\right|}\right]$$

$$F_a(\theta) = \frac{1}{2N}e^{-j\left[\frac{N-1}{2}\right](\theta-\theta_0)}\left[\frac{\left|\sin\left[\frac{N}{2}(\theta-\theta_0)\right]\right|}{\left|\sin\left[\frac{1}{2}(\theta-\theta_0)\right]\right|}\right] + \frac{1}{2N}e^{-j\left[\frac{N-1}{2}\right](\theta+\theta_0)}\left[\frac{\left|\sin\left[\frac{N}{2}(\theta+\theta_0)\right]\right|}{\left|\sin\left[\frac{1}{2}(\theta+\theta_0)\right]\right|}\right] +$$

$$\frac{(1+\epsilon)}{2N}e^{-j\left[\frac{N-1}{2}\right](\theta-\theta_0)}\left[\frac{\left|\sin\left[\frac{N}{2}(\theta-\theta_0)\right]\right|}{\left|\sin\left[\frac{1}{2}(\theta-\theta_0)\right]\right|}\right] - \frac{(1+\epsilon)}{2N}e^{-j\left[\frac{N-1}{2}\right](\theta+\theta_0)}\left[\frac{\left|\sin\left[\frac{N}{2}(\theta+\theta_0)\right]\right|}{\left|\sin\left[\frac{1}{2}(\theta+\theta_0)\right]\right|}\right]$$

END

DATE

FILMED

11-88

DTIC